

Soft Physics at the LHC

Masterarbeit

von

Patrick Kirchgaßer

am Institut für Theoretische Physik
der Fakultät für Physik

Referent: PD. Dr. S. Gieseke

Korreferent: Prof. Dr. D. Zeppenfeld

November 2016

Hiermit versichere ich, dass ich die vorliegende Arbeit selbständig verfasst und keine anderen als die angegebenen Hilfsmittel benutzt, die wörtlich oder inhaltlich übernommenen Stellen als solche kenntlich gemacht und die Satzung des Karlsruher Instituts für Technologie (KIT) zur Sicherung guter wissenschaftlicher Praxis in der aktuell gültigen Fassung beachtet habe.

Karlsruhe, den 21. November 2016

.....

(Patrick Kirchgaeßer)

Als Masterarbeit anerkannt.

Karlsruhe, den 21. November 2016

.....

(PD. Dr. S. Gieseke)

Contents

| | |
|--|-----------|
| 1. Introduction | 1 |
| 2. Prerequisites | 3 |
| 2.1. QCD Lagrangian | 3 |
| 2.2. Asymptotic freedom and confinement | 4 |
| 2.3. Regge theory | 5 |
| 3. Monte Carlo event generators | 9 |
| 3.1. Hard scattering process | 9 |
| 3.2. Parton shower | 10 |
| 3.2.1. Single branching | 11 |
| 3.2.2. Multiple branchings | 12 |
| 3.2.3. Initial state showering | 13 |
| 3.2.4. Shower algorithms | 14 |
| 3.3. Hadronisation | 15 |
| 3.3.1. Gluon splitting and cluster formation | 15 |
| 3.3.2. Cluster fission | 16 |
| 3.3.3. Cluster and particle decays | 18 |
| 4. Multiple parton interactions | 21 |
| 4.1. Semi-hard interactions | 21 |
| 4.2. Soft interactions | 23 |
| 4.3. Implementation | 25 |
| 5. Multiperipheral particle production | 29 |
| 5.1. Multiperipheral kinematics | 30 |
| 5.2. Implementation | 35 |
| 5.3. Tuning | 39 |
| 5.3.1. General tuning procedure | 40 |
| 5.3.2. Tuning to minimum bias data | 41 |

| | |
|---|-----------|
| 5.4. Results | 42 |
| 5.4.1. Rapidity gap analysis | 43 |
| 5.4.2. Analysis of non-single-diffractive events | 46 |
| 5.4.3. Extrapolation to 13 TeV | 47 |
| 5.5. Conclusion | 48 |
| 6. Colour reconnection | 49 |
| 6.1. Colour reconnection models in Herwig 7 | 50 |
| 6.1.1. Plain colour reconnection | 52 |
| 6.1.2. Statistical colour reconnection | 53 |
| 6.1.3. Effect of colour reconnection on the new softMPI model | 53 |
| 6.2. Extensions to colour reconnection | 53 |
| 6.2.1. Algorithm | 57 |
| 6.3. Tuning | 57 |
| 6.3.1. Tuning to hadron colliders | 58 |
| 6.4. Results | 61 |
| 6.4.1. Rapidity gap analysis | 62 |
| 6.4.2. Analysis of non-single-diffractive events | 63 |
| 6.4.3. Baryon ratios | 63 |
| 6.5. Conclusion | 64 |
| 7. Summary and outlook | 67 |
| Bibliography | 69 |
| A. Tuning | 75 |
| B. Eikonal approximation | 79 |

1. Introduction

The goal of modern particle physics is to strive towards a more sound understanding of nature. One big step in that direction was achieved with the discovery of the Higgs boson at the Large Hadron Collider (LHC) in 2012, the last missing piece of the Standard Model of particle physics. In order to open the doors for future discoveries, improvements of theoretical predictions and an understanding of all aspects of hadronic collisions are essential.

In this regard Monte Carlo event generators play an important role. They simulate the outcome of particle collisions which can be compared to data measured in experiments at the LHC. Large parts of the event generation depend on perturbative calculations. These high precision calculations are limited to a regime in which perturbation theory is valid. Many aspects of the event generation fall outside that regime and have to be modeled by theoretical considerations and phenomenological constraints. One example is hadronisation which describes the transition from quarks and gluons to hadrons. Another example is the simulation of the underlying event. Hadrons are composite objects made of quarks and gluons. During a collision there can be several interactions among the constituents. Experimental observations indicate that more than one pair of partons may interact during one hadronic collision. These additional interactions are called multiple parton interactions and contribute significantly to the underlying event. These interactions typically occur at smaller transverse momenta than the main hard interaction but still lie within the perturbative regime. In order to describe multiple parton interactions outside the perturbative regime, so called soft interactions, non-perturbative models have to be applied.

In the first part of this thesis we implement a new model for such soft multiple parton interactions, based on the ideas from Regge theory, in the Monte Carlo event generator Herwig 7 [1]. In the second part we investigate and implement additional possibilities of colour reconnection as an extension to the hadronisation model applied in Herwig 7.

Both models are fully compatible with Herwig 7 and can be seen as an extension and alternative to already existing models.

Ch. 2 explains theoretical concepts with a focus on strong interactions and outlines the ideas behind Regge theory. The next chapter explains the different steps of the simulation of a particle collision with the event generator Herwig 7. In Ch. 4 we introduce multiple parton interactions in the context of Herwig 7 and Ch. 5 covers the implementation and analysis of the new model for soft multiple parton interactions. In Ch. 6 we investigate colour reconnection and discuss the implemented extensions to the model before we summarise the findings of this work and give a brief outlook on future topics in Ch. 7.

2. Prerequisites

This thesis deals with the implementation of non-perturbative models in the event generation of Herwig 7 [1]. In order to embed these models in the overall picture of particle physics we give a brief outline of particle physics theory. Until the success of quantum field theories it was tried to describe the interactions among particles in a non-perturbative framework called *Regge theory* [2]. Regge theory can be seen as a complementary approach to the subject and many of its ideas and results are of crucial importance in particle physics. In modern elementary particle physics the *Standard Model* (SM) is used to describe the fundamental interactions of particles. The SM is the combination of two quantum field theories, *Quantum Chromodynamics* (QCD) and the electroweak theory. It describes all known fundamental particles and correctly postulated the existence of the Higgs boson which was discovered at the LHC in 2012 [3, 4]. QCD describes the elementary interactions among partons such as quarks and gluons. Observed in nature are hadrons which originate from these elementary processes at the parton level. The formation of hadrons happens at the soft scale $Q_0 \approx \mathcal{O}(1 \text{ GeV})$ where perturbation theory is not valid anymore and cannot be understood from first principles. In order to describe non-perturbative effects they have to be modeled based on phenomenological considerations.

In Sec. 2.1 and 2.2 we discuss the behaviour of the QCD Lagrangian which describes the physics of strong interactions at different energy scales. In Sec. 2.3 we outline the ideas behind Regge theory and explain its importance for modern particle physics.

2.1. QCD Lagrangian

Here we discuss the component of the Standard Model that describes the theory of strong interactions. The QCD Lagrangian is based on the non-abelian $SU(3)_C$ gauge group and is given by

$$\mathcal{L}_{\text{QCD}} = \sum_{\Psi=u,d,s,\dots} \bar{\Psi}(iy^\mu D_\mu - m_\Psi)\Psi - \frac{1}{4}F^{a\mu\nu}F_{\mu\nu}^a + \mathcal{L}_{\text{gauge}} + \mathcal{L}_{\text{ghost}} , \quad (2.1)$$

where D_μ is the covariant derivative

$$D_\mu = \partial_\mu - ig_s T^a G_\mu^a, \quad (2.2)$$

and Ψ are the massive quark fields which transform under $SU(3)_C$ as colour triplets $\Psi = (\Psi_1, \Psi_2, \Psi_3)$. The field strength tensor $F_{\mu\nu}^a$ is given by

$$F_{\mu\nu}^a = \partial_\mu G_\nu^a - \partial_\nu G_\mu^a + g_s f^{abc} G_\mu^b G_\nu^c, \quad (2.3)$$

where g_s is the strong coupling constant and G_μ^a are the eight massless gluon fields which correspond to the eight $SU(3)_C$ generators T^a . The f^{abc} are the structure constants defined by the commutator relations of the generators of the $SU(3)_C$ group,

$$[T^a, T^b] = if^{abc} T^c. \quad (2.4)$$

In the fundamental representation of $SU(3)_C$ the eight generators are the Gell-Mann matrices $T_{ij}^a = \frac{\lambda_{ij}^a}{2}$.

In order to define the gluon propagator a particular gauge choice has to be made which is done via the gauge fixing term $\mathcal{L}_{\text{gauge}}$. The term $\mathcal{L}_{\text{ghost}}$ is a complex scalar field which is needed to cancel unphysical degrees of freedom that would otherwise propagate in covariant gauges.

The first term in Eq. (2.1) describes the kinetic energy of the quarks and the interactions with the gluons. It is important to note that the flavour of the quarks is not changed by the gluons. In contrast to abelian gauge theories self interactions between gluons are contained in the terms proportional to $F_{\mu\nu}^2$ which lead to asymptotic freedom.

2.2. Asymptotic freedom and confinement

Asymptotic freedom [5, 6] means that the coupling of the strong interaction $\alpha_s = g_s^2/4\pi$ becomes small at high energies or short distances. This scale dependence of the coupling is expressed by the *Renormalisation Group Equation* (RGE),

$$\beta(\alpha_s) = Q^2 \frac{d\alpha_s}{dQ^2}. \quad (2.5)$$

In this equation β can be expanded as a power series in α_s ,

$$\beta(\alpha_s(Q^2)) = -\alpha_s(Q^2)^2 (b_1 + b_2 \alpha_s(Q^2) + \dots), \quad (2.6)$$

where $b_1 = \frac{33-2n_f}{12\pi}$, $b_2 = \frac{153-19n_f}{24\pi^2}$ and the variable n_f is the number of active flavours. In QCD n_f is typically ≤ 6 which leads to a vanishing coupling constant at asymptotically large energies which is called asymptotic freedom. If the expansion of the β function in Eq. (2.6) is truncated after the quadratic term α_s^2 the solution to Eq. (2.5) reads

$$\alpha_s(Q^2) = \frac{\alpha_s(\mu^2)}{1 + \alpha_s(\mu^2)b_1 \ln\left(\frac{Q^2}{\mu^2}\right)}. \quad (2.7)$$

The value of the coupling constant α_s cannot be calculated but has to be measured. A typical choice for μ is the pole mass of the Z -boson $\mu^2 = M_Z^2$. The coupling at this scale has been measured to be $\alpha_s(M_Z^2) \approx 0.12$. With this value for $\alpha_s(M_Z^2)$ Eq. (2.7) exceeds unity for $Q^2 < \mathcal{O}(0.1 - 1 \text{ GeV})$ and perturbation theory can no longer be applied. Another parametrisation of Eq. (2.7) is

$$\alpha_s(Q^2) = \frac{1}{b_1 \ln \frac{Q^2}{\Lambda_{\text{QCD}}^2}}, \quad (2.8)$$

where Λ_{QCD} is a dimensionful parameter which depends on the renormalisation scheme and the order in which the β function is computed. This equation defines the scale where the coupling constant diverges. Perturbation theory is only valid for values of Q^2 much larger than Λ_{QCD}^2 . For a 4-loop beta function in the $\overline{\text{MS}}$ scheme it has the value $\Lambda_{\text{QCD}}^{\overline{\text{MS}}} = 220 \text{ MeV}$. Note: In 2016 α_s was calculated at 5-loop accuracy in Ref. [7].

Experimental observations indicate that the only observed states are colour singlet states under $SU(3)_C$, namely mesons and baryons. This phenomenon is called (*colour confinement*).

2.3. Regge theory

Before strong interactions were considered in a field theoretical approach, Regge theory was used very successfully in describing the scattering of strongly interacting particles [2, 8]. The starting point is the partial wave expansion of the amplitude for a two body scattering process $a + b \rightarrow c + d$,

$$\mathcal{A}(s, t) = \sum_{l=0}^{\infty} (2l+1) a_l(t) P_l\left(1 + \frac{2s}{t}\right), \quad (2.9)$$

where a_l are the partial wave amplitudes, P_l are the Legendre polynomials and the index l denotes the orbital angular momentum. Eq. (2.9) can be converted to a contour integral

in the complex angular momentum plane using the Sommerfeld-Watson transformation [8]. In the *Regge limit*, where $s \gg |t|$ the amplitude vanishes for $|l| \rightarrow \infty$ where the asymptotic behaviour of the Legendre polynomial was exploited in order to extract the high energy behaviour of the scattering amplitude. In this limit only the sum over the residues of the Regge poles at $l_k = \alpha_k(t)$ remain and the Legendre polynomials can be approximated by $(\frac{2s}{t})^l$. Only the leading Regge pole with the largest value of the real part of $\alpha(t)$ has to be considered which leads to a power-like behaviour of the amplitude,

$$\mathcal{A}(s, t) \xrightarrow{s \rightarrow \infty} \beta(t)\eta(t)s^{\alpha(t)}, \quad (2.10)$$

where the position of the leading Regge pole is denoted by $\alpha(t)$. The function $\beta(t)$ is the residue and $\eta(t)$ is the signature factor which is given by

$$\eta(t) = -\frac{1 + \tau e^{-i\pi\alpha(t)}}{\sin i\alpha(t)}. \quad (2.11)$$

Amplitudes for t -channel processes with positive t are expected to have poles corresponding to the exchange of physical particles of spin j and mass m , $\alpha(t = m^2) = j$. In Ref. [9] it was found that by plotting light mesons against their square mass the relationship between spin j and squared mass m^2 is linear,

$$\alpha(t) = \alpha(0) + \alpha' t. \quad (2.12)$$

This function $\alpha(t)$ is called *Regge trajectory* or *Reggeon* where $\alpha(0)$ is the intercept and α' the slope of the Reggeon. With the values of $\alpha(0)$ and α' the asymptotic behaviour of Eq. (2.10) is defined.

With the optical theorem the asymptotic behaviour of the total cross section σ_{tot} can be calculated from a given Regge amplitude such as Eq. (2.10). The total cross section for that process reads,

$$\sigma_{\text{tot}} \approx \frac{1}{s} \Im \mathcal{A}(s, t = 0) \propto s^{\alpha(0)-1}. \quad (2.13)$$

From the values that were obtained for the trajectory of ρ -mesons in Ref. [9] follows,

$$\alpha(t) = 0.55 + 0.86 \text{ GeV}^{-2} t. \quad (2.14)$$

With these values the total cross section (Eq. (2.13)) decreases with s . In Ref. [10] Pomernichuk proved from general assumptions that the cross section vanishes asymptotically for any process in which charge is exchanged. In experiments, on the other hand, it was

observed that the total cross section rises slowly as s increases. In order to attribute the rise of the total cross section to a Regge trajectory, a Reggeon with intercept $\alpha(0) > 1$ and quantum numbers of the vacuum has to be considered. This trajectory is named *Pomeron* and denoted by \mathbb{P} . It is therefore concluded that the trajectory of the Pomeron dominates the scattering amplitude at high energies. In Ref. [11] Donnachie and Landshoff parameterised the total cross section of pp and $p\bar{p}$ collisions in terms of Reggeon and Pomeron trajectories. According to this parameterisation the pomeron intercept has the value $\alpha_{\mathbb{P}}(0) = 1.0808$. In Ref. [12, 13] it is shown that a Pomeron exchange can be interpreted as ladders of particles. Final state particles corresponding to a Pomeron exchange are strongly ordered in rapidity. This interpretation of the Pomeron will be the basis for the implementation of the new model for soft multiple parton interactions which will be described in detail in Ch. 5.

We also quickly outline the connection between Pomeron exchanges and the eikonal formalism upon which the model for multiple parton interactions of Herwig 7 is based. The amplitude for n -pomeron exchanges can be written in terms of the born amplitude [14]

$$\mathcal{A}^{(n)}(s, b) = \frac{1}{2i} \frac{(-\chi(s, b))^n}{n!}, \quad (2.15)$$

where $\chi(s, b) = -2i\mathcal{A}^{(1)}(s, b)$ is the eikonal function. It can be shown that the cross section for exactly k cut Pomerons in the eikonal model reads

$$\sigma_k(s) = \int d^2b \frac{(2\chi)^k}{k!} \exp(-2\chi). \quad (2.16)$$

The inelastic cross section can be calculated by adding up all cross sections with at least one pomeron exchanged,

$$\sigma_{\text{inel}}(s) = \sum_{k=1}^{\infty} \sigma_k(s) = \int d^2b (1 - e^{-2\chi}). \quad (2.17)$$

With the total cross section,

$$\sigma_{\text{tot}}(s) = 2 \int d^2b (1 - e^{-\chi}), \quad (2.18)$$

it follows for the elastic cross section

$$\sigma_{\text{el}}(s) = \int d^2b (1 - e^{\chi})^2, \quad (2.19)$$

2. Prerequisites

and at small momentum transfer the hadronic elastic scattering cross section can be parameterised by

$$\frac{d\sigma_{el}(t)}{dt} \approx \left[\frac{d\sigma_{el}}{dt} \right]_{t=0} e^{-B_{el}|t|}, \quad (2.20)$$

where B_{el} is the elastic slope parameter. In the eikonal model the slope of the elastic cross section is given by [15]

$$B_{el}(s, t = 0) = \frac{1}{\sigma_{tot}(s)} \int d^2b (1 - e^\chi). \quad (2.21)$$

3. Monte Carlo event generators

Herwig 7 [1] is a multi-purpose Monte Carlo event generator that simulates high-energy particle collisions. The simulation needs to cover all aspects of the collision between particles, including the hard scattering process, the parton shower, multiple scattering between partons and the hadronisation of particles. The different steps of a simulation for a pp collision are shown in Fig. 3.1. The hadronic cross section for the scattering of two partons a and b into n final states is calculated according to

$$\sigma_{\text{QCD}} = \sum_{a,b} \int_0^1 dx_a dx_b \int d\Phi_n f_a^{h_1}(x_a, \mu_F) f_b^{h_2}(x_b, \mu_F) \times \frac{1}{2s} |M_{ab \rightarrow n}|^2(\Phi_n; \mu_F; \mu_R) \quad (3.1)$$

× Hadronisation,

where $f_a^h(x, \mu)$ is the PDF which states the probability of finding a parton a with momentum fraction x inside its parent hadron h at energy scale μ_F . The squared matrix element $|M_{ab \rightarrow n}|^2(\Phi_n; \mu_F; \mu_R)$ denotes all allowed processes as a sum of Feynman diagrams that can happen in the hard scattering process and $d\Phi_n$ denotes the differential phase space element for n -particles appearing in the final state.

While the hard scattering process and the parton shower are based on perturbation theory one has to rely upon models in order to simulate the hadronisation and the transition from the unstable particles to the particles that can be observed in the detector.

This chapter gives an overview about the different steps of the event generation with Herwig 7. The generation of the hard scattering process is explained in Sec. 3.1. Sec. 3.2 describes the physics and the algorithms that are used to simulate the parton shower and Sec. 3.3 covers the hadronisation model.

3.1. Hard scattering process

One of the key components of an event generator is the generation of the hard scattering process with high transverse momentum transfer between the involved particles. While the determination of the matrix element at e^+e^- collisions is relatively straightforward,

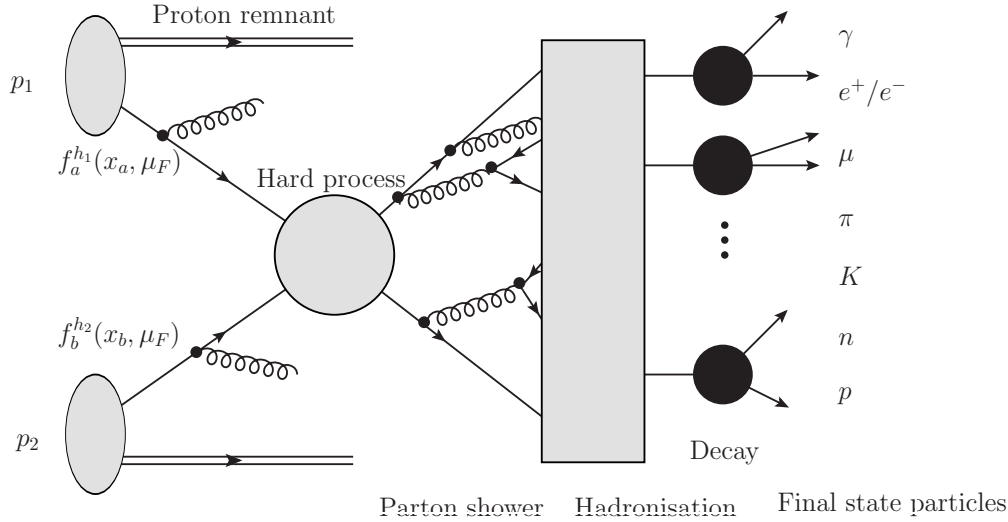


Figure 3.1.: Shown is a sketch of all parts that contribute to the hadronic cross section in a pp collision. The flavour and the momenta of incoming partons are chosen according to proton PDFs. The hard process produces the primary outgoing fundamental particles, the parton shower evolves the energy of these particles down to the hadronic scale by radiating off particles and the hadronisation describes the formation of hadrons out of quarks and gluons, which then proceed to decay into the observed final state particles.

the fact that hadrons itself are composite objects makes the calculation of cross sections at hadron colliders such as the LHC a very complicated venture. At a pp collision, the flavour, the momenta and the partons who are involved in the collision have to be determined via *Parton Distribution Functions* (PDFs).

In Herwig 7 the user can decide which processes to take into account. A limited selection of matrix elements is already implemented in the library of Herwig 7 and with an interface to external matrix element providers like MadGraph [16] or VBFNLO [17] it is possible to include more matrix elements than the default ones. A standard format for the exchange of data between different programs is specified by the *Les Houches Accord* [18].

3.2. Parton shower

In Herwig 7 the hard scattering process is calculated up to Next-to-leading order (NLO) QCD. Some Next-to-Next-to-leading order (NNLO) corrections are available but beyond that the complexity of the calculation grows exponentially. The parton shower approximation resums the effects of higher order corrections of perturbative QCD. It starts at the energy scale of the hard scattering process Q^2 and evolves the particles down to the

hadronisation scale $Q_0^2 \sim 1 \text{ GeV}$. Two different shower algorithms are implemented in Herwig 7, the angular ordered \tilde{q} -shower and the dipole shower which can be used as an alternative.

3.2.1. Single branching

In order to outline a formula for additional parton radiation we start with the cross section for the process $e^+e^- \rightarrow q\bar{q} = \sigma_{q\bar{q}}$ which can be calculated to leading order in perturbation theory. The differential cross section for the next-to-leading-order process, $e^+e^- \rightarrow q\bar{q}g = \sigma_{q\bar{q}g}$, where one of the quarks emits a gluon is given by [19]

$$\frac{d\sigma_{q\bar{q}g}}{d\cos\theta dz} \approx \sigma_{q\bar{q}} C_F \frac{\alpha_s}{2\pi} \frac{2}{\sin^2\theta} \frac{1+(1-z)^2}{z}, \quad (3.2)$$

where C_F is the colour factor. In Eq. (3.2) we see that the cross section $\sigma_{q\bar{q}g}$ is proportional to the leading order process $\sigma_{q\bar{q}}$. The rest of the equation can be interpreted as the probability for additional gluon emission. Eq. (3.2) has the following divergences:

- $\theta \rightarrow 0$ which means that the emitted gluon is collinear to the quark,
- $\theta \rightarrow \pi$ which means that the gluon is back to back to the quark and collinear to the antiquark,
- $z \rightarrow 0$ the energy of the emitted gluon is going to zero.

First we focus on the collinear region where $\theta \rightarrow 0$ or $\theta \rightarrow \pi$. The term that is responsible for the divergence can be written as the sum of two distributions that are describing the divergence for one of the two collinear regions,

$$\frac{2}{\sin^2\theta} \approx \frac{1}{1-\cos\theta} + \frac{1}{1-\cos\bar{\theta}}, \quad (3.3)$$

where $\bar{\theta}$ describes the angle between the gluon g and the antiquark \bar{q} . With this separation the differential cross section can be written as the sum over independent emission distributions for each parton,

$$d\sigma_{q\bar{q}g} \approx \sigma_{q\bar{q}} \sum_{\text{partons}} \frac{\alpha_s}{2\pi} \frac{d\theta^2}{\theta^2} dz \frac{1+(1-z)^2}{z}, \quad (3.4)$$

where we have picked the opening angle θ between the gluon and the quark as the ordering variable. Other phase space parameterisations with variables that are proportional

to θ lead to a mathematically-identical expression. Other used parameterisations are the virtuality of the off-shell quark propagator q^2 , or the transverse momentum of the gluon k_\perp^2 . Because of

$$\frac{d\theta^2}{\theta^2} = \frac{dq^2}{q^2} = \frac{dk_\perp^2}{k_\perp^2} \quad (3.5)$$

these expressions lead to an identical result up to the leading logarithmic approximation. It can be shown that the structure of Eq. (3.4) is completely general. The differential cross section of any hard process with cross section σ_0 for parton i with an additional parton j that has momentum fraction z is given by

$$d\sigma \approx \sigma_0 \sum_{\text{partons},i} \frac{\alpha_s}{2\pi} \frac{d\theta^2}{\theta^2} dz P_{ji}(z, \phi) d\phi, \quad (3.6)$$

where $P_{ji}(z, \phi)$ are flavour and in general spin-dependent functions called the *splitting functions*. The spin-averaged splitting functions $P_{ji}(z, \phi)$ are given by,

$$\begin{aligned} P_{qq}(z) &= \frac{4}{3} \frac{1+z^2}{1-z}, \\ P_{gq}(z) &= \frac{4}{3} \frac{1+(1-z)^2}{z}, \\ P_{gg}(z) &= 3 \frac{z^4 + 1 + (1-z)^4}{z(1-z)}, \\ P_{qg}(z) &= \frac{1}{2} (z^2 + (1-z)^2). \end{aligned} \quad (3.7)$$

Eq. (3.6) can be used to write an iterative algorithm. The first step is to use it on the hard process and generate one splitting. Treat the splitting as the new hard process and then generate more splittings. At this stage the divergences are still not accounted for. The absolutely collinear splitting where both partons fly in the same direction has no actual physical effect. They cannot be distinguished from a single parton with the same quantum numbers by any physical measurement. Therefore it is reasonable to produce only distributions of resolvable partons above some cutoff scale Q_0 . This cuts off the soft and collinear divergences and gives a resolvable finite emission probability.

3.2.2. Multiple branchings

In order to calculate multiple branchings we pick the virtuality of the internal quark propagator q^2 as the ordering variable. The factor multiplied to σ_0 in Eq. (3.6) can then be seen as the probability for the emission of a parton of type i in the energy range q^2

and $q^2 + dq^2$,

$$d\mathcal{P}_i = \frac{\alpha_s}{2\pi} \frac{dq^2}{q^2} \int_{Q_0^2/q^2}^{1-Q_0^2/q^2} dz P_{ji}(z), \quad (3.8)$$

where the limits on z come from the condition that the emitted partons have to be resolvable. The probability of having no resolvable branching between the scales Q_0 and Q is called the *Sudakov form factor* and has the form,

$$\Delta_i(Q^2, Q_0^2) = \exp \left\{ - \int_{Q_0^2}^{Q^2} \frac{dk^2}{k^2} \frac{\alpha_s}{2\pi} \int_{Q_0^2/k^2}^{1-Q_0^2/k^2} dz P_{ji}(z) \right\}. \quad (3.9)$$

The Monte Carlo implementation of the parton shower is based on the Sudakov form factor. According to Ref. [19] one possibility to calculate the scale q' at which the next branching is happening is to choose a random number R between $[0, 1]$ and solve the equation

$$\Delta_i(Q^2, q'^2) = R \quad (3.10)$$

for q' . If $q'^2 > Q_0^2$ a branching is generated at scale q'^2 and the z value is chosen according to $P_{ij}(z)$. If the value of q'^2 is lower than the cutoff scale Q_0^2 the evolution is terminated. The algorithm is then applied recursively for each of the products of the branching.

3.2.3. Initial state showering

Apart from final state radiation one also has to consider the showering of the particles before the hard collision takes place. In Monte Carlo event generators initial state radiation is extremely inefficient because the correct kinematics are needed in order to produce a certain hard process of interest. The usual way how the simulation of initial state radiation is handled is that the event generation starts by selecting a hard process and then uses the parton shower algorithm to add additional radiation. In order to simulate initial state radiation the Sudakov form factor (Eq. (3.9)) from the final state shower is replaced by a Sudakov form factor which explicitly depends on the PDFs of the colliding hadrons,

$$\Delta_i(Q^2, q^2; x) = \exp \left\{ - \int_{Q_0^2}^{Q^2} \frac{dk^2}{k^2} \frac{\alpha_s}{2\pi} \int_{Q_0^2/k^2}^{1-Q_0^2/k^2} dz P_{ji}(z) \frac{x/z f_j(x/z, k^2)}{x f_i(x, k^2)} \right\}. \quad (3.11)$$

The evolution takes the correct probability to find a particular flavour with the sampled values of momentum fraction and scale q into account. The emitted partons from the initial state shower will go on to produce final state parton showers.

With the extra factor in Eq. (3.11) the parton shower will terminate mostly at a stage where a valence (anti-)quark has been produced. Their PDFs dominate at high x and low Q^2 . If the parton shower does not terminate on a valence (anti-)quark, additional branchings are performed in order to force that a valence quark is extracted from the hadron.

3.2.4. Shower algorithms

Two shower algorithms are implemented in Herwig 7. The angular ordered \tilde{q} -shower and the dipole shower.

3.2.4.1. Angular-ordered shower

In order to simulate the angular ordered shower, Herwig 7 uses the coherent branching algorithm derived in Ref. [20]. The evolution scale is the variable \tilde{q} defined as,

$$\tilde{q} = \frac{2E_a^2(1 - \cos \theta_{bc})(1 + \cos \theta_a)^2}{(1 + \cos \theta_b)(1 + \cos \theta_c)}, \quad (3.12)$$

for branchings $a \rightarrow bc$ where θ_b and θ_c are the angles between the children b, c and the shower progenitor a . θ_a is the angle between parent a and its shower progenitor and E_a denotes the energy of parent a . For small emission angles the evolution variable can be approximated as

$$\tilde{q} \approx E_a \theta_{bc}. \quad (3.13)$$

As long as no gluons are involved the initial condition of the colour flow is unique. In order to treat the colour information of gluons in the event a random choice is made between the two possible configurations of colour lines.

3.2.4.2. Dipole shower

In the $N_c \rightarrow \infty$ limit [21] the colour structure of the event can be decomposed in a set of colour lines. Each colour line connects a coloured parton with an anticoloured parton and forms a colour-anticolour dipole. The shower is then generated according to the dipole radiation pattern of a pair of partons. Each dipole splits into two new dipoles when it emits a gluon. These dipoles can split again until some cutoff Q_0^2 is reached and the shower is terminated. Each emission with a finite transverse momentum results in a recoil of the system. Since a gluon carries both colour and anticolour and is thereby connected to two dipoles, the recoil may affect the subsequent evolution of neighbour-

ing dipoles. In order to prevent that, the emission of the highest transverse momentum from any dipole is generated first and this transverse momentum gives the upper limit for the following evolution of dipoles. The total emission probability is the sum of the two splitting functions each associated with one leg of the colour-anticolour dipole. The implementation of the dipole shower is based on the Catani-Seymour subtraction kernel [22].

3.3. Hadronisation

After the parton shower perturbatively splitted the partons in the event from the scale of the hard interaction Q^2 down to some infrared cutoff scale Q_0^2 a model is required that converts the partons to hadrons at the energy scale of Λ_{QCD} . In Herwig 7 this is done via the cluster model [23]. The cluster model is based on the preconfinement property of the angular-ordered parton shower [24], which states that the colour structure of the parton shower at any scale Q_0^2 is such that colour singlet combinations of partons can be formed with an asymptotically invariant mass distribution. The mass distribution of the colour singlets is independent of the properties of the hard scattering process or the parton shower itself.

In the $N_c \rightarrow \infty$ limit the colour structure of a QCD shower can be represented on a plane as a set of colour lines each connecting a coloured parton with an anticoloured parton [21]. In this limit the gluons in the shower carry both colour and anticolour and are connected to two other partons. The remaining gluons are split non-perturbatively into quark-antiquark pairs and clusters are then formed from colour connected quarks and antiquarks. Clusters that are too heavy in order to decay directly into hadrons are fissioned into cluster pairs and the resulting clusters decay into excited hadrons which successively decay into the observed particles. The whole event, ranging from the hard process to the decay of the clusters into final state particles including colour lines is depicted in Fig. 3.2 for a e^+e^- collision.

3.3.1. Gluon splitting and cluster formation

The gluons that are left once the parton shower has terminated are split non-perturbatively into quark-antiquark pairs where only the light flavours, up, down and strange are allowed with different weights. For the splitting into quarks the gluon needs to have at least twice the mass of the lightest quark $m_g > 2m_q$. The splitting $g \rightarrow q\bar{q}$ is done isotropically in the rest frame of the gluon. After the gluon splitting the event only contains

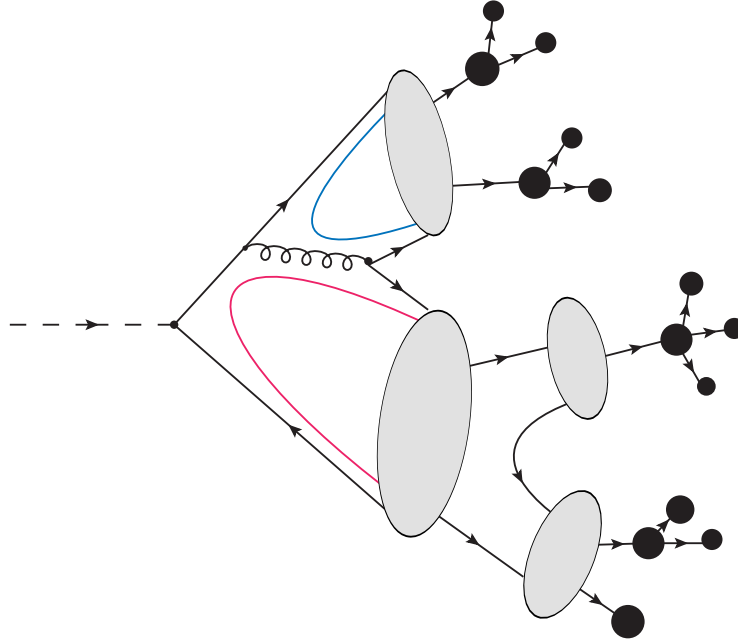


Figure 3.2.: Sketch of a whole process as simulated by Herwig. Shown is the Z -Boson from the e^+e^- collision at $\sqrt{s} = 91$ GeV. The clusters are formed from colour connected quarks and antiquarks which fission into smaller clusters and decay into final state particles.

colour connected quarks and antiquarks. These colour connected quark pairs are formed into colourless singlets, called clusters where the momenta of the clusters is calculated as the sum of the momenta of the constituents $p_C = \sum_i p_i$. From now on we refer to the clusters that are formed from partons that originate from the parton shower as primary clusters.

According to the preconfinement property [24] the invariant mass of these clusters is independent of the hard scattering process, the centre-of-mass energy or the parton shower and the distribution of the clusters peaks at low invariant masses of the order $\mathcal{O}(1 - 3 \text{ GeV})$. For e^+e^- collisions at $\sqrt{s} = 91.2 \text{ GeV}$ the invariant mass distribution of the primary clusters is shown in Fig. 3.3 and we see that the preconfinement property is satisfied fairly well.

3.3.2. Cluster fission

The primary clusters can be seen as highly excited hadron resonances which decay according to the allowed phase space and flavour of the constituents into the observed hadrons.

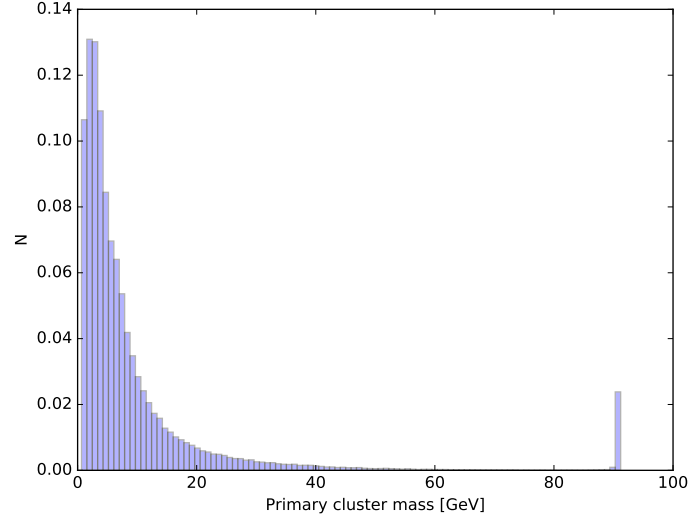


Figure 3.3.: Invariant mass distribution of primary clusters from a e^+e^- collision at $\sqrt{s} = 91.2$ GeV. The distribution peaks at small masses and has a long tail towards higher masses. The peak at ~ 91 GeV comes from events without initial- or final state radiation.

In Fig. 3.3 we see that there is a small fraction of clusters that is too heavy to decay directly into hadrons. These clusters need to be split into lighter clusters before they can decay. The condition to decide whether a cluster needs to undergo fission is

$$M^{\text{Cl}_{\text{pow}}} \geq \text{Cl}_{\text{max}}^{\text{Cl}_{\text{pow}}} + (m_1 + m_2)^{\text{Cl}_{\text{pow}}}, \quad (3.14)$$

where M is the invariant mass of the cluster and m_1, m_2 are the masses of the constituent quarks. Cl_{pow} and Cl_{max} are free parameters of the model which have different values for different quark flavours. If Eq. (3.14) is satisfied a light quark-antiquark pair is created from the vacuum where the flavour is again selected only from light quarks. The fission of one cluster of mass M into two lighter clusters of respective masses M_1 and M_2 is shown in Fig. 3.4. Once the quark flavour is selected the original cluster with mass M fissions into two new clusters with one of the original quarks in each of the new clusters. The masses of the two new clusters are chosen according to

$$\begin{aligned} M_1 &= m_1 + (M - m_1 - m_q)\mathcal{R}^{1/P}, \\ M_2 &= m_2 + (M - m_2 - m_q)\mathcal{R}^{1/P}, \end{aligned} \quad (3.15)$$

where m_q is the mass of the quark from the vacuum, $M_{1,2}$ are the masses of the two new clusters after the fission and P controls the distribution of cluster masses according to which the masses are sampled. Again P has distinct values for different quark flavours.

The configuration of new cluster masses M_1 and M_2 is accepted if the sum of the new cluster masses is smaller than the original cluster mass, $M_1 + M_2 \leq M$, and the sum of the constituent masses of the new clusters is less than the mass of the new clusters.

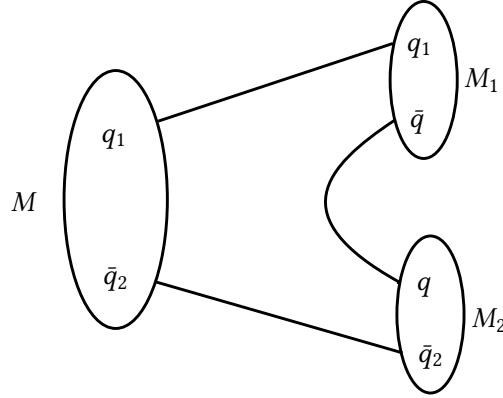


Figure 3.4.: Cluster fission of a parent cluster of mass M into two child clusters of masses M_1 and M_2 . The quarks q and \bar{q} are sampled from light flavour quarks (u, d, s) and have the same mass.

If one of the clusters contains a particle from the beam remnant in a hadronic collision the mass of the two new clusters is sampled from an exponential distribution

$$M_i = m_i + m_q + x , \quad (3.16)$$

where x is sampled between 0 and $M - m_1 - m_2 - 2m_q$ according to

$$\frac{dP}{dx^2} = e^{-bx} , \quad (3.17)$$

where b determines the slope of the mass distribution.

3.3.3. Cluster and particle decays

Once all heavy clusters are fissioned, the clusters decay into pairs of excited hadrons, where the type of the hadrons depends on the available phase space, the flavour and the spin of the constituents.

After the decay products are determined by the properties of the cluster, the cluster decays isotropically in its rest frame. A cluster that contains a parton from the perturbative

stage of the event retains the direction of that parton but undergoes a Gaussian smearing, where the polar angle is sampled via

$$\cos \theta_{\text{smr}} = 1 + \text{Cl}_{\text{smr}} \log(\mathcal{R}) , \quad (3.18)$$

Cl_{smr} is a free parameter distinct for different quark flavours. The azimuthal angle ϕ is distributed uniformly between 0 and 2π . If the cluster is too light in order to decay into two new hadrons, it decays into the lightest allowed hadron instead. Energy and momentum is reshuffled between neighbouring clusters in order to give the hadron the correct physical mass. The hadrons that originate from cluster decays are excited hadron states which decay into the final state particles that can be observed in the detector.

4. Multiple parton interactions

In order to fully describe the collision between hadrons additional activity in one hadron collision has to be considered. This additional source of hadronic activity is known as the *underlying event*. From the experimental point of view the underlying event is defined as everything that is not related to the hard scattering process of the collision. For large centre-of-mass energies the probability of having more than one partonic interaction accompanying the main hard scattering becomes significant. These interactions are modeled as *multiple parton interactions* and are the dominant contribution to the underlying event at high energies.

The currently used model to simulate multiple parton interactions is based on the eikonal model from Refs. [25, 26, 27, 28]. It consists of a perturbative part and a non-perturbative part where the non-perturbative part has been introduced in Ref. [29]. Multiple parton interactions are modeled as perturbative and non-perturbative scatterings between gluons. We differ between the two types depending on their transverse momentum: *i)* The interactions above a certain transverse momentum p_{\perp}^{\min} are simulated as QCD $2 \rightarrow 2$ processes and are referred to as *semi-hard* interactions. *ii)* Below p_{\perp}^{\min} the interactions are modeled as elastic gluon scatterings and are referred to as *soft* interactions. With this model it was possible to show reasonable results when applied to underlying event or minimum bias data [30], but it failed in some other aspects which will be discussed in Ch. 5. In this chapter we summarise the physics and the implementation of the multiple parton interaction model used in the current version of Herwig 7. For a more detailed description we refer to the Herwig++ manual [31] and to App. B where we show the eikonal approximation for a quantum mechanical amplitude.

4.1. Semi-hard interactions

The cross section for inclusive jet production $\sigma_{\text{jet}}^{\text{inc}}$ can be calculated within perturbative QCD. The hadronic cross section rises with centre-of-mass energy s because of the high values of the PDFs at small momentum fractions x . The calculated cross section may exceed the total pp or $p\bar{p}$ cross section already at intermediate energies as it was shown

in Ref. [32]. This seemingly violation of unitarity is resolved by interpreting the jet cross section as the inclusive jet cross section $\sigma_{\text{hard}}^{\text{inc}}$ in respect of the luminosity of the incoming partons [25]. The jet cross section exceeds the total cross section by a factor equal to the mean multiplicity of multiple interactions. If per collision $\langle n_{\text{dijet}} \rangle$ jet pairs are produced on average with transverse momentum larger than p_{\perp}^{min} , we have

$$\sigma_{\text{hard}}^{\text{inc}}(s, p_{\perp}^{\text{min}}) = \langle n_{\text{dijet}} \rangle \cdot \sigma_{\text{inel}}(s, p_{\perp}^{\text{min}}), \quad (4.1)$$

where σ_{inel} is the cross section for having one or more jet pairs above p_{\perp}^{min} .

In Ref. [25] it was shown that the effects of unitarisation corrections can be modeled in an eikonal formalism through the appearance of multiple parton scatterings.

The cross sections for multiple parton scatterings can be calculated within an eikonal model. With the eikonal approximation it is possible to relate the cross section for hadron-hadron collisions to the more elementary interactions among these partons. One approach followed by Durand and Pi [26, 28] determines the total and elastic cross sections using the eikonal formalism in terms of the average number of elementary interactions $\langle n(b, s) \rangle$ at fixed impact parameter $\mathbf{b} = b$ and centre-of-mass energy s .

The model assumes that at fixed impact parameter b the individual interactions are independent of each other. Furthermore it uses the simplification that the distribution of partons within hadrons factorises in terms of b and the longitudinal momentum fraction x . Note: There are other approaches that propose PDF's that are dependent of the impact parameter presented in Ref. [33]. Such an approach is implemented in Pythia in Ref. [34] but is not pursued here since the models implemented in Herwig 7 rely on the assumptions from Refs. [35, 25]. Following Refs. [26, 28] the average number of elementary interactions, $\langle n(b, s) \rangle$, in a hadron-hadron collision is given by

$$\langle n(b, s) \rangle = A(b) \sigma_{\text{hard}}^{\text{inc}}(s, p_{\perp}^{\text{min}}), \quad (4.2)$$

where σ_{hard} is the inclusive cross section for hard interactions above a minimum value for the transverse momentum p_{\perp}^{min} and $A(b)$ describes the overlap of the two colliding hadrons. The overlap function $A(b)$ must satisfy

$$\int d^2b A(b) = 1. \quad (4.3)$$

Assuming that the PDFs of the overlapping hadrons factorise in terms of x and b and estimating the b dependent functions using the electromagnetic form factors of the proton

results in the following parameterisation of the overlap function,

$$A(b, \mu) = \frac{\mu^2}{96\pi} (\mu b)^3 K_3(\mu b), \quad (4.4)$$

where K_3 is the modified Bessel function of the third kind. Assuming further that the different interactions are uncorrelated leads to a Poissonian distribution for the average number of hard interactions given by Eq. (4.2)

$$P_k = \frac{\langle n(b, s) \rangle^k}{k!} \exp(-\langle n(b, s) \rangle). \quad (4.5)$$

The cross section for jet production due to k uncorrelated interactions is the Poissonian from Eq. (4.5) integrated over the impact parameter space.

$$\sigma_k(\sigma_{\text{hard}}^{\text{inc}}) = \int d^2b P_k(A(b, \mu) \cdot \sigma_{\text{hard}}^{\text{inc}}) = \int d^2b \frac{(A(b, \mu) \cdot \sigma_{\text{hard}}^{\text{inc}})^k}{k!} e^{-A(b, \mu) \sigma_{\text{hard}}^{\text{inc}}}. \quad (4.6)$$

If one compares this cross section with the cross section for k cut Pomerons (Eq. (2.16))

$$\sigma_k(s) = \int d^2b \frac{(2\chi)^2}{k!} \exp(-2\chi), \quad (4.7)$$

from Sec. 2.3 the two formulas coincide if the eikonal is chosen as

$$\chi_{\text{hard}}(s, b) = \frac{1}{2} A(b, \mu) \sigma_{\text{hard}}^{\text{inc}}(s, p_{\perp}^{\text{min}}), \quad (4.8)$$

and one can conclude that multiple hard interactions correspond to cut pomerons in the eikonal formalism. At large centre-of-mass energies, s , and small interaction lengths, the probability that a gluon carrying a small momentum fraction x is involved in the scattering process increases rapidly according to the PDF. This means that multiple parton interactions will most likely involve the scattering of gluons off each other. The additional semi-hard interactions are implemented as gluon scatterings according to the QCD matrix element with $p_{\perp} > p_{\perp}^{\text{min}}$. From these semi-hard gluons, parton showers are generated.

4.2. Soft interactions

In Ref. [36] it was shown that the semi-hard model for multiple parton interactions was able to describe underlying event data from Tevatron when the leading jet has a p_{\perp} higher than 20 GeV. The model however failed to describe low- p_{\perp} jet production and minimum

bias analyses, where a low cut on the transverse momentum is applied. The apparent reason for this was the lacking of partonic interactions below p_{\perp}^{\min} .

In Ref. [30] the semi-hard model was extended to the soft regime $p_{\perp} < p_{\perp}^{\min}$ where perturbation theory is no longer valid.

Following Refs. [28, 35, 26], the starting point is to generalise the eikonal formalism to include soft interactions, where the total eikonal function χ_{tot} is taken as the sum of a hard eikonal function χ_{hard} and a soft eikonal function χ_{soft} ,

$$\chi_{\text{tot}}(b, s) = \chi_{\text{hard}}(b, s) + \chi_{\text{soft}}(b, s), \quad (4.9)$$

where the hard part has the same form as in Eq. (4.8)

$$\chi_{\text{hard}} = \frac{1}{2} A(b, \mu) \sigma_{\text{hard}}^{\text{inc}}(s) \quad (4.10)$$

and the soft part is given by

$$\chi_{\text{soft}} = \frac{1}{2} A_{\text{soft}}(b, \mu_{\text{soft}}) \sigma_{\text{soft}}^{\text{inc}}(s), \quad (4.11)$$

where σ_{soft} is the non-perturbative cross section for soft interactions below p_{\perp}^{\min} . The simplest choice is to assume, that the soft overlap function A_{soft} has the same structure as A_{hard} in Eq. (4.10) but depends on the parameter μ_{soft} . In analogy to Eq. (4.7) the cross section of having exactly h semi-hard and n soft interactions is given by

$$\sigma_{h,n}(s) = \int d^2b \mathcal{P}_{h,n}(b, s), \quad (4.12)$$

where $\mathcal{P}_{h,n}$ is generalised to the cross section for h semi-hard and n soft uncorrelated interactions,

$$\mathcal{P}_{h,n} = \frac{2\chi_{\text{hard}}(b, s)^h}{h!} \frac{2\chi_{\text{soft}}(b, s)^n}{n!} e^{-2\chi_{\text{tot}}(b, s)}. \quad (4.13)$$

The parameter μ_{soft} is dynamically fixed to describe the elastic t -slope from Eq. (2.21) correctly at the used centre-of-mass energy. The other parameter of the soft model, σ_{soft} , cannot be calculated by perturbation theory, instead σ_{soft} is chosen such that the total cross section that was obtained by the parameterisation of Ref. [11] is correctly described.

4.3. Implementation

The soft interactions are modeled as elastic scatterings among gluons. The generation of the additional soft interactions starts once all perturbative evolution has terminated. After the hard process and the parton shower the number of additional interactions is calculated according to Eq. (4.13). While the semi-hard interactions are generated as gluonic QCD $2 \rightarrow 2$ scatterings, the soft interactions are implemented as a non-perturbative remnant decay. The gluons are radiated from the two remnants that remain after the hard scattering was simulated and are elastically scattered off each other as shown in Fig. 4.1.

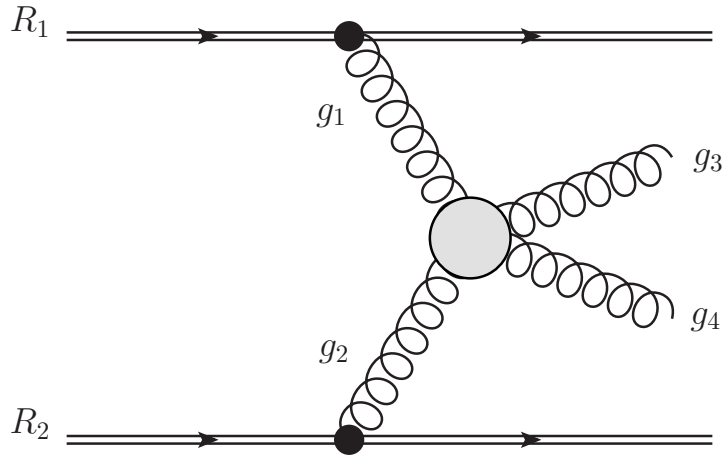


Figure 4.1.: Picture of the simulation of soft a elastic scattering of gluons that get radiated off the hadron remnant R_1 and R_2 .

The four-momenta in the lab frame of the incoming gluons is given by

$$p_{g_{1,2}}^\mu = \left(\sqrt{\frac{x_{1,2}^2 s}{4} + m_g^2}, 0, 0, \pm \sqrt{\frac{x_{1,2}^2}{s} 4} \right)^T, \quad (4.14)$$

where s is the centre-of-mass energy, m_g is the gluon mass and $x_{1,2}$ is the longitudinal momentum fraction of the gluon. The four-momenta of the incoming gluons is entirely determined by $x_{1,2}$ which is sampled according to a $f(x) = 1/x$ distribution between x_{\min} and x_{\max} , where x_{\min} is an arbitrary cutoff to exclude the singularity at 0 and x_{\max} is the maximum available energy in the hadron remnant. The four-momenta of the outgoing gluons can be parameterised in the centre-of-mass frame by

$$p_{g_{1,2}}^\mu = \left(\sqrt{p_\perp^2 + p_z^2 + m_g^2}, \pm p_\perp \cos \phi, \pm p_\perp \sin \phi, p_z \right)^T, \quad (4.15)$$

where the transverse momentum p_{\perp} is sampled below p_{\perp}^{\min} from a distribution that is parameterised with a Gaussian distribution according to

$$\frac{d\sigma_{\text{soft}}^{\text{inc}}}{dp_{\perp}^2} = Ae^{-\beta p_{\perp}^2}. \quad (4.16)$$

The two parameters A and β of the Gaussian distribution are fixed by two constraints:

i) The soft cross section has to match the total soft cross section which was fixed to describe σ_{tot}^1 and the elastic slope parameter b_{el} of Eq. (2.21)

$$\int dp_{\perp}^2 \frac{d\sigma_{\text{soft}}^{\text{inc}}}{dp_{\perp}^2} \stackrel{!}{=} \sigma_{\text{soft}}^{\text{inc}}. \quad (4.17)$$

ii) The differential transverse momentum distribution has to match the perturbative distribution at $p_{\perp} = p_{\perp}^{\min}$

$$\left. \frac{d\sigma_{\text{hard}}^{\text{inc}}}{dp_{\perp}^2} \right|_{p_{\perp}=p_{\perp}^{\min}} \stackrel{!}{=} \left. \frac{d\sigma_{\text{soft}}^{\text{inc}}}{dp_{\perp}^2} \right|_{p_{\perp}=p_{\perp}^{\min}}. \quad (4.18)$$

The azimuthal angle ϕ is sampled from a uniform distribution $\phi \in (0, 2\pi)$ and with p_{\perp} , the longitudinal momentum p_z is fixed by momentum conservation

$$p_z^2 = \frac{(p_{g_1} + p_{g_2})^2}{4} - p_{\perp}^2 - m_g^2. \quad (4.19)$$

After the kinematics are generated in the centre-of-mass frame the gluons are boosted back to their corresponding lab frames and then the remnant momenta are reshuffled such that they remain on their original mass shell. After successful reshuffling of momenta, the available energy for the next soft interaction is determined and the process is iterated until the requested number of soft interactions is reached or there is no more energy available in the remnants.

In Fig. 4.2 we show the two possible colour connections for two soft interactions. A line with an arrow to the right corresponds to a colour line and a line with an arrow to the left is an anticolour line. Gluons are depicted with the colour and the anticolour line. The remnants always have anticolour. Either the gluons are connected to each other or the gluons are connected to the remnant were one colour line is automatically connected to the previous process, which can be e.g the hard scattering or a previous soft interaction.

¹In the new model σ_{tot} also includes diffractive events.

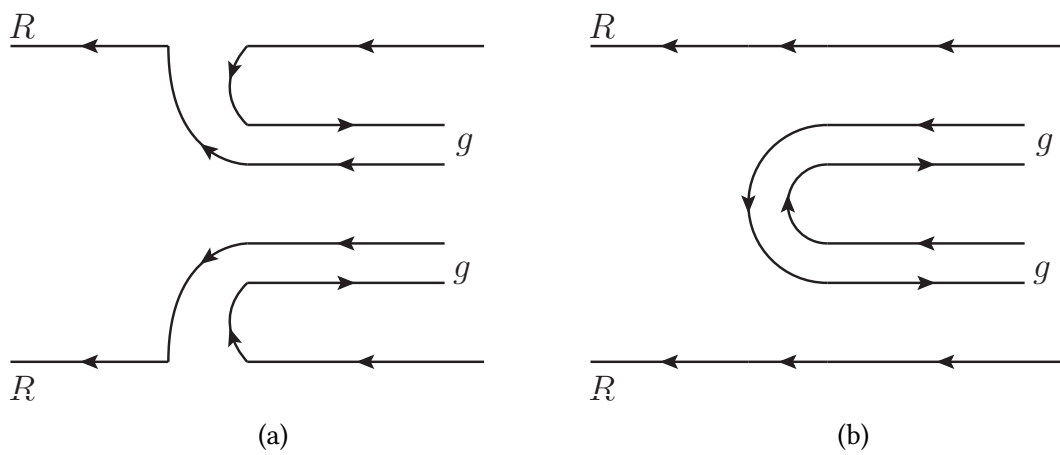


Figure 4.2.: Shown are the two possible colour connections between the gluons and the remnants. A colour line is depicted as an arrow to the right while an anti-colour line is depicted as an arrow to the left. The gluons can be connected to the remnant (a) or they can be connected to each other (b). In the first case one colour line of the gluon may be connected with an anti colour line of a previous soft interaction or a different part of the process like the hard scattering process.

5. Multiperipheral particle production

The soft model for multiple particle interactions (see Sec. 4.2) was implemented in order to describe the soft part of the underlying event for low- p_{\perp} jet production. It also achieved good results in describing minimum bias data from Tevatron [30]. Nevertheless the model has some shortcomings when extrapolated to higher energies and compared to LHC data: While it was shown that a systematic re-tuning of the parameters of the multiple parton interaction model in combination with a model for colour reconnection indeed resulted in a better description of minimum bias data [37, 38], it leads to an enhancement in the large pseudorapidity gap region $\Delta\eta$ [39, 40]. This is certainly a flaw of the used model, since Herwig 7 had no implementation of diffraction which is responsible for the main contribution to the large $\Delta\eta$ region. Probing all possible colour connections between the gluons and the beam remnants in order to reduce the amount of events with large rapidity gaps resulted in a small decrease but none of the considered topologies was able to produce the required fall off that is necessary to describe the non-diffractive part of the data correctly [39]. By separately running the semi-hard and the soft model we found out that the soft model for multiple parton interactions is responsible for the increase of the cross section in the large $\Delta\eta$ region. Therefore we propose a fundamental change to the model in order to describe the non-diffractive part of the cross section correctly. The model we propose should have two main properties: *i)* From minimum bias analyses it is known that the distribution of soft particles is approximately uniform in rapidity in the kinematic range available. *ii)* The non-diffractive part of the cross section should be proportional to $e^{-a\Delta\eta}$ where a is some a priori unknown constant. In Ref. [13] it was shown that these features can be described by a model with *multiperipheral particle production*. When incorporating this model into Herwig 7 small changes have to be made in order to account for the specific peculiarities of the event generator but the idea and the physics stay the same.

This chapter is organised as follows. The model for multiperipheral particle production and the kinematic implications are discussed in Sec. 5.1. The implementation of the model in Herwig 7 is explained in Sec. 5.2. In Sec. 5.3 we tune the parameters of the model to

minimum bias data and in Sec. 5.4 we show the results of the tuning procedure with cross checks to other analyses.

5.1. Multiperipheral kinematics

The model we implemented in Herwig 7 is inspired by the model for multiperipheral particle production presented in Ref. [13]. Multiperipheral particle production is a $2 \rightarrow N$ process where the N resulting particles are ordered in rapidity. In Ref. [13] it was shown that multiperipheral particle production can be achieved when three main features are incorporated into the model:

- i) The produced particles are ordered in rapidity.
- ii) The momenta of the produced particles are correlated.
- iii) The sub-energies $s_{i,i+1} = (p_i + p_{i+1})^2$ are of the order $\mathcal{O}(\text{GeV})$. Large $s_{i,i+1}$ correspond to diffractive processes.

Note: The second part of point iii) does not apply to our implementation because we model the multiperipheral particle production as non-perturbative gluon emissions. A large subenergy $s_{i,i+1}$ between the gluons would correspond to a large cluster which will lead to a high multiplicity. Diffractive processes are taken care of by the diffraction model from Ref. [39]. A process with multiperipheral particle production is shown in Fig. 5.1. p_A and p_B are the incoming particles that interact with each other and the p_i are the outgoing particles. The internal "virtual" particles are denoted by q_i . In the following we will refer to a $2 \rightarrow N$ process with multiperipheral particle production as a *particle ladder*. The goal of this section is to investigate the kinematic properties of the particle ladder and derive some relations that will be useful for the implementation of this model in Herwig 7.

In order to investigate the kinematic properties, it is instructive to separate the momenta in a transverse $p_{i\perp}$ and a longitudinal component p_{iz} . Hence we write for internal momenta q_i and for external momenta p_i

$$\mathbf{p}_i = (p_{i\perp}, p_{iz}) , \quad (5.1)$$

$$\mathbf{q}_i = (q_{i\perp}, q_{iz}) . \quad (5.2)$$

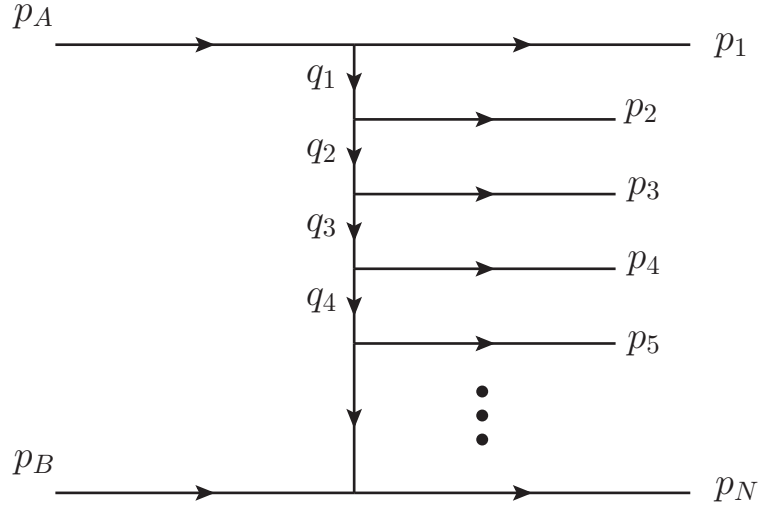


Figure 5.1.: Graph of a multiperipheral amplitude.

The energies are

$$E_i = \sqrt{m_i^2 + p_{i\perp}^2 + p_{iz}^2}, \quad (5.3)$$

$$\omega_i = \sqrt{q_i^2 + q_{i\perp}^2 + q_{iz}^2}. \quad (5.4)$$

In high energy particle collisions almost all particles move in a narrow cone along the collision axis which is defined as the z -axis of the collision. Due to the large centre-of-mass energy $\sqrt{s} \gg m$ most particles are ultrarelativistic. Therefore it is reasonable to assume that the longitudinal component of the momentum is large compared to the transverse component,

$$p_{iz}^2 \gg m_i^2 + p_{i\perp}^2, \quad (5.5)$$

$$q_{iz}^2 \gg q_i^2 + q_{i\perp}^2, \quad (5.6)$$

and

$$|q_i^2| \sim p_{i\perp}^2 \sim q_{i\perp}^2 \sim m^2. \quad (5.7)$$

5. Multiperipheral particle production

The energies can be written as

$$E_i \approx |p_{iz}| + \frac{m_i^2 + p_{i\perp}^2}{2|p_{iz}|}, \quad (5.8)$$

$$\omega_i \approx |q_{iz}| + \frac{q_i^2 + q_{i\perp}^2}{2|q_{iz}|}. \quad (5.9)$$

It is convenient to use light cone variables [41], where the light cone coordinates are defined by a change of variables that explicitly depend upon the choice of the z-axis. These coordinates show nicely the small and large components of the momentum. In high energy particle collisions there is a natural choice of the z-axis, the collision axis. For the momenta \mathbf{p}_i and \mathbf{q}_i the light cone coordinates are defined as

$$p_{i+} := E_i + p_{iz}, \quad p_{i-} := E_i - p_{iz}, \quad (5.10)$$

$$q_{i+} := \omega_i + q_{iz}, \quad q_{i-} := \omega_i - q_{iz}. \quad (5.11)$$

With the Eqs. (5.5-5.9) the light cone coordinates can be written as

$$p_{i+} = 2p_{iz}, \quad p_{i-} = \frac{m_i^2 + p_{i\perp}^2}{2p_{iz}}, \quad (5.12)$$

$$q_{i+} = 2q_{iz}, \quad q_{i-} = \frac{q_i^2 + q_{i\perp}^2}{2q_{iz}}. \quad (5.13)$$

With these formulas we can describe the kinematics of the splitting processes in the multiperipheral particle ladder. The splitting for one virtual state q_i is shown in Fig. 5.2. The virtual state q_i splits into one particle p_{i+1} and one virtual state q_{i+1} ,

$$q_i \rightarrow q_{i+1} + p_{i+1}. \quad (5.14)$$

The momentum fraction which is given to p_{i+1} and q_{i+1} is defined by the variable x_{i+1} . In terms of light cone coordinates this is described by,

$$q_{i,+} \rightarrow q_{i+1,+} + p_{i+1,+} = x_{i+1}q_{i,+} + (1 - x_{i+1})q_{i,+}. \quad (5.15)$$

With Eqs. (5.12) and (5.13) this can be written in terms of longitudinal momenta,

$$x_{i+1} = q_{i+1z}/q_{i,z} = 1 - p_{i+1z}/q_{i,z}. \quad (5.16)$$

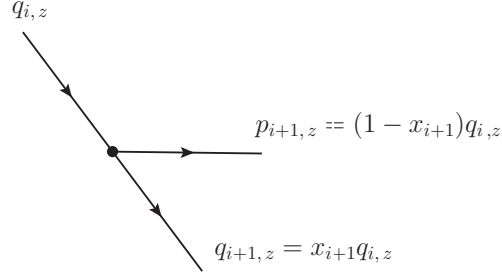


Figure 5.2.: Splitting of one virtual state q_i . The particle p_{i+1} and the virtual state q_{i+1} are each getting a fraction of the longitudinal momentum of the virtual state q_i .

In order to account for momentum conservation it is clear that the sum of the longitudinal momentum of particle p_{i+1} and the virtual state q_{i+1} must be equal to the longitudinal momentum of the virtual state q_i

$$q_{i,z} = p_{i+1,z} + q_{i+1,z} \quad (5.17)$$

$$\Rightarrow q_{i,z} - q_{i+1,z} = p_{i+1,z} \stackrel{!}{>} 0. \quad (5.18)$$

It follows that the momentum q_i , carried away by the $(i + 1)$ -th virtual state, has to be smaller than the momentum q_i of the i -th virtual state

$$q_{i,z} > q_{i+1,z}. \quad (5.19)$$

This can be expressed as an ordering of the z -component of the momenta of the virtual states q_i

$$q_{0z} = p_{Az} > q_{1z} > q_{2z} > \dots > q_{N-1,z} > q_{Nz} = -p_{Bz}, \quad (5.20)$$

where q_N is the last particle in the ladder which is equal to p_B . All p_{iz} can be written in terms of x_i which was defined in Eq. (5.16),

$$\begin{aligned} p_{1z} &= (1 - x_1)p_{Az}, \\ p_{2z} &= (1 - x_2)x_1 p_{Az}, \\ &\vdots \\ p_{iz} &= (1 - x_i)x_{i-1}\dots x_2 x_1 p_{Az}, \end{aligned} \quad (5.21)$$

5. Multiperipheral particle production

and also all q_{iz}

$$\begin{aligned}
 q_{1z} &= x_1 p_{Az} , \\
 q_{2z} &= x_2 x_1 p_{Az} , \\
 &\vdots \\
 q_{iz} &= x_i x_{i-1} \dots x_2 x_1 p_{Az} .
 \end{aligned} \tag{5.22}$$

For $i = N$ in Eq. (5.22), it follows that p_{B+} is the product of

$$p_{B+} = -q_{N+} = - \left[\prod_{i=1}^N x_i \right] p_{A+} . \tag{5.23}$$

If we assume that the momentum fractions x_i for each splitting are roughly equal with an average value of $\langle x_i \rangle \sim 1/C$, where C is some constant, the average number of particles $\langle N \rangle$ in one multiperipheral ladder follows from Eq. (5.23) in the lab frame of particle B [13],

$$C^{\langle N \rangle} = \frac{p_{A+}}{p_{B+}} = \frac{s}{m_B^2} , \tag{5.24}$$

where we used $p_{A+} = s/m_B$ and $p_{B+} = m_B$. Taking the logarithm on both sides and sorting for $\langle N \rangle$, this equation leads to a formula for the average number of particles per ladder,

$$\langle N \rangle = \frac{1}{\ln C} \ln \left(\frac{s}{m_B^2} \right) . \tag{5.25}$$

Another useful relation can be obtained when taking the rapidity of the i -th particle into account. With Eqs. (5.12) the rapidity of particle i can be written as,

$$y_i = \frac{1}{2} \ln \left(\frac{E_i + p_{iz}}{E_i - p_{iz}} \right) = \frac{1}{2} \ln \left(\frac{p_{i+}}{p_{i-}} \right) = \ln \frac{2p_{i+}}{m_{i\perp}} = \ln \frac{4p_{iz}}{m_{i\perp}} . \tag{5.26}$$

where $m_{i\perp} = \sqrt{m_i^2 + p_{i\perp}^2}$ is the transverse momentum of particle i . For every particle p_i produced in the ladder the longitudinal momentum decreases. If we assume that the transverse mass remains approximately constant, $m_{i\perp} \sim m_{i+1,\perp} \sim \text{const.}$, the rapidity (5.26) decreases with each produced particle. The condition (5.20) translates then directly into an ordering in terms of rapidity of the produced particles,

$$y_1 > y_2 > \dots > y_{N-1} > y_N . \tag{5.27}$$

The picture we have now is that the colliding particles p_A and p_B result in a $2 \rightarrow N$ process where the N particles are ordered in rapidity.

For two consecutive particles within the ladder, the rapidity difference $\Delta y_{i,i+1}$ is calculated according to,

$$\begin{aligned}
 \Delta y_{i,i+1} &= y_i - y_{i+1} \\
 &= \ln \left(\frac{2p_{i+}}{m_{i\perp}} \right) - \ln \left(\frac{2p_{i+1,+}}{m_{i+1,\perp}} \right) \\
 &= \ln \left(\frac{p_{i+}}{p_{i+1,+}} \right) + \ln \left(\frac{m_{i+1,\perp}}{m_{i\perp}} \right) \\
 &\approx \ln \left(\frac{p_{i+}}{p_{i+1}} \right),
 \end{aligned} \tag{5.28}$$

where we assumed that $m_{i\perp} \approx m_{i+1,\perp} \approx \text{const.}$ and $x_i \approx x_{i+1} \approx x \approx \text{const.}$. In combination with Eq. (5.21), Eq. (5.28) results in a very simple form for the rapidity difference between two neighbouring particles within one ladder,

$$\Delta y_{i,i+1} \approx \ln \left(\frac{(1-x)x^i p_{A+}}{(1-x)x^{i+1} p_{A+}} \right) = \ln \left(\frac{1}{x} \right) = \Delta y. \tag{5.29}$$

The total rapidity difference ΔY between the incoming particles A and B can be calculated in a similar manner,

$$\Delta Y \approx \ln \left(\frac{p_{A+}}{p_{B+}} \right) = \ln \left(\frac{s}{m_B} \right). \tag{5.30}$$

With Eq. (5.29) where $\Delta y_{i,i+1} \approx \text{const.} \approx \Delta y$, we can express ΔY in terms of the number of particles in one ladder,

$$(N + 1)\Delta y = \Delta Y. \tag{5.31}$$

Combining Eqs. (5.29) and (5.30) leads to a formula for the average momentum fraction x ,

$$x = e^{-\frac{\Delta Y}{(N+1)}}. \tag{5.32}$$

If x would be chosen exactly as in Eq. (5.32) the N particles will be distributed equally in rapidity.

5.2. Implementation

This section describes the implementation of the multiperipheral model in Herwig 7. In order to interfere as little as possible with other parts of the event generator we keep the structure of the old model for multiple parton interactions as explained in Ref. [42]. The

multiperipheral model is entirely implemented as a decay of the hadron remnants that are left after the hard scattering process. To simulate minimum bias events the hard scattering is implemented as a toy process to trigger the decay of the beam remnants. This is implemented as a fictitious dummy process between two quarks with no momentum and no colour transfer. The semi-hard part of the old model for multiple parton interactions is preserved while the multiperipheral particle production replaces the previous soft part. The number of soft interactions, N_{soft} , that are calculated from Eq. (4.13) are treated as particle ladders in the new model. Assuming that the number of particles in each ladder is uncorrelated, we sample the number of particles ($N_{\text{poissonian}}$) from a Poissonian distribution around N_{avg} , where N_{avg} is obtained from Eq. (5.25). We note that the number of particles in the ladder decreases with the production of every new ladder because the remaining energy in the remnants decreases which leads to a smaller N_{avg} in Eq. (5.25). The generation of ladders continues until N_{soft} ladders are produced or until the number of particles in the ladder is zero. In Fig. 5.4a we show the difference between the calculated number of ladders N_{soft} and the actual number of ladders N_{ladder} , that were generated. We see that in almost every case N_{soft} equals N_{ladder} .

The kinematics of the particles in the ladder is then generated as a splitting process from Eq. (5.21). Here we explain the general procedure for the generation of the kinematics in the first ladder as an example.

For minimum bias events the 'hard' scattering process is modeled as a toy process with as little effect as possible as explained in Ref. [31]. Only light quarks are extracted from the hadrons and they are scattered with no exchange of momentum and no exchange of colour. The longitudinal momentum fraction of the quarks is determined by x_{min} . In order to get a valence-like distribution we arbitrarily set the value to $x_{\text{min}} = 0.11^1$. The remaining longitudinal momenta of the hadronic remnants is then

$$\begin{aligned} p_{A,z} &= (1 - x_{\text{min}}) p_{\text{Beam},1} , \\ p_{B,z} &= (1 - x_{\text{min}}) p_{\text{Beam},2} . \end{aligned} \tag{5.33}$$

The extraction of a quark has no effect on the direction of the beam remnant. Therefore $p_{A/B,\perp} = 0$. After the scattering the extracted quarks are colour connected to the respective remnants. The number of soft interactions are calculated according to Eq. (4.12) and the number of particles in the first ladder are sampled from a Poissonian distribution around N_{avg} from Eq. (5.25).

¹The value is also motivated by the requirement that we want the extracted quark and the remnant to have roughly the same rapidity because they remain colour connected and form a cluster.

The kinematics of the particles in the ladder is implemented as a stepwise splitting process from both remnants p_A and p_B similar to Sec. 4.3. This is shown in Fig. 5.3, where the indices A, B indicate from which remnant the particles originate.

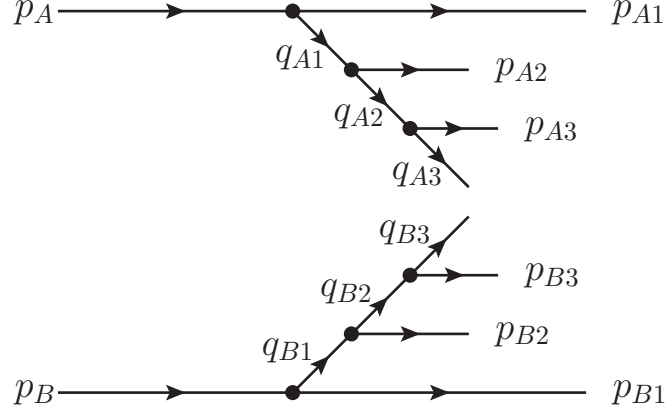


Figure 5.3.: Emission of a ladder of soft particles from the beam remnants p_A and p_B . The emission is simulated as a splitting process from the two remnants. p_{A1} and p_{B1} are the remaining remnants from which the next ladder is produced.

The remnants are split into the first particles in the ladder p_{A1}, p_{B1} and the virtual states q_{A1}, q_{B1} ,

$$\begin{aligned} p_A &\rightarrow q_{A1} + p_{A1} , \\ p_B &\rightarrow q_{B1} + p_{B1} . \end{aligned} \quad (5.34)$$

The total four-momenta of $p_{A1}, p_{B1}, q_{A1}, q_{B1}$ are calculated according to

$$\begin{aligned} p_{A1} &= (1 - x_1) p_A \quad q_{A1} = x_1 p_A , \\ p_{B1} &= (1 - x_1) p_B \quad q_{B1} = x_1 p_B , \end{aligned} \quad (5.35)$$

where x_1 is sampled from a Gaussian distribution around the calculated x from Eq. (5.32). The simplest choice is to use the same x for both splittings in Eq. (5.35). Next we chose a mass $m = m_{A1} = m_{B1}$ for the virtual particles². The following steps are all performed in the centre-of-mass frame of the two virtual states q_{A1} and q_{B1} . The transverse momentum of the virtual states, $p_{\perp} = q_{A1, \perp} = q_{B1, \perp}$, is sampled from a Gaussian distribution that is parameterised as explained in Ch. 4.3 as,

$$\frac{d\sigma_{\text{soft}}^{\text{inc}}}{dp_{\perp}^2} = A e^{-\beta p_{\perp}^2} , \quad (5.36)$$

²Here we also need to rescale the energy in order not to violate energy-momentum conservation.

5. Multiperipheral particle production

where the upper limit of p_{\perp} is given by p_{\perp}^{\min} and the azimuthal angle which defines the direction of p_{\perp} is sampled uniformly between 0 and 2π . With the total four-momentum $q_{A1/B1}$, the mass m_q and the transverse momentum p_{\perp} , the longitudinal momentum of the virtual states $q_{A1,z} = q_{B1,z} = p_z$ is fixed by energy-momentum conservation in the centre-of-mass frame,

$$p_z = \sqrt{\frac{(q_{A1} + q_{B1})^2}{4} - p_{\perp}^2 - m_q^2}. \quad (5.37)$$

Once the kinematic is defined, the virtual states q_{A1}, q_{B1} are split into the second particles in the ladder p_{A2}, p_{B2} and the next virtual states q_{A2}, q_{B2} . This procedure is repeated until the calculated number of particles, $N_{\text{poissonian}}$, is reached or until there is no more energy available in the virtual states. Due to momentum conservation the momentum of the last two particles from each remnant, $q_{A/B,i}$ and $p_{A/B,i}$ are of the same order if $x \approx 0.5$. Note that the first particles in the ladder are the remaining remnants from which the next ladder is generated. At every new splitting process the conservation of energy is checked with

$$q_i < (1 - x_{i+1})q_i + x_{i+1}q_i. \quad (5.38)$$

Energy-momentum conservation might be violated because x is sampled from a Gaussian distribution and the term $\ln(\frac{m_{i\perp}}{m_{i+1,\perp}})$ is neglected in Eq. (5.28). If conservation of energy-momentum is violated the step is rejected and tried again until a maximum number of tries is reached. Once the maximum tries are exceeded, the ladder is intercepted.

In Fig. 5.4b we show the difference between the calculated number of particles from the Poissonian distribution and the actual number of particles that are created in the ladder and see that in $\sim 80\%$ of ladders, all particles are created.

Once all particles are produced or the ladder gets intercepted the colour connections are set according to Fig. 5.5. Each arrow represents a colour line and in order to form clusters each colourline has to be connected to an anticolour line. Note that the first two virtual states have to be quarks in order to get the correct colour connections. All following particles are gluons. A gluon carries both, colour and anticolour and is connected to two other partons. The proton remnants are connected to the hard scattering part of the event. With this algorithm we generate N_{soft} ladders with colour connected particles ordered equally in rapidity.

The only new parameter in this model is a factor n_{Ladder} that we introduce in Eq. (5.25)

$$\langle N \rangle = n_{\text{Ladder}} \ln\left(\frac{s}{m_B^2}\right), \quad (5.39)$$

which calculates the number of particles in the ladder. This parameter steers the production of more smaller clusters that are closer in rapidity or less larger clusters.

In order to explain the data and the whole cross section available correctly the new model for soft interactions is combined with the diffraction model from Ref. [39]. For simplicity we refer to the combination of the new model for soft multiple parton interactions and the model for diffraction as the "softMPI" model.

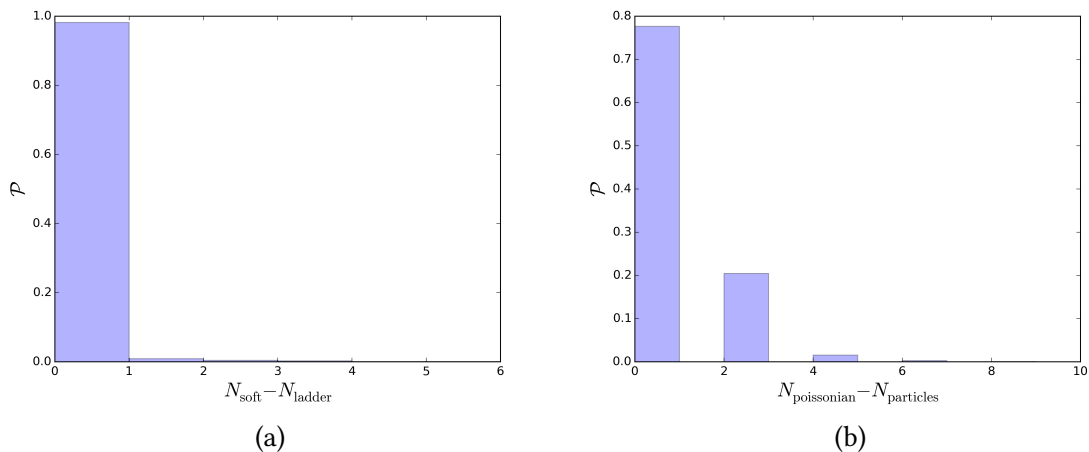


Figure 5.4.: (a) Comparison between the number of soft interactions and the number of ladders created. (b) Difference between the number of particles calculated by the Poissonian and actually created in the ladder for $\sqrt{s} = 7$ TeV. We obtain similar results for $\sqrt{s} = 900$ GeV.

5.3. Tuning

In the last section we described the implementation of a new model for the production of soft multiple parton interactions. Here we tune the free parameters of the model to a small set of minimum bias observables at $\sqrt{s} = 900$ GeV and $\sqrt{s} = 7$ TeV centre-of-mass energy using the current version of the PROFESSOR tuning software [43]. All analyses were done with the help of Rivet [44]. The tuning results in two slightly different sets of parameters for 900 GeV and 7 TeV. The difference can be seen as an energy dependence of the model. We refer to the different sets of parameters as MB-900 and MB-7. With the tuned parameters we find an overall better description for the observables which were tuned to as well as for all other observables of the minimum bias analysis which were not considered in the tuning procedure. The description improves significantly compared to the old model. The new model is also able to describe observables from other analyses

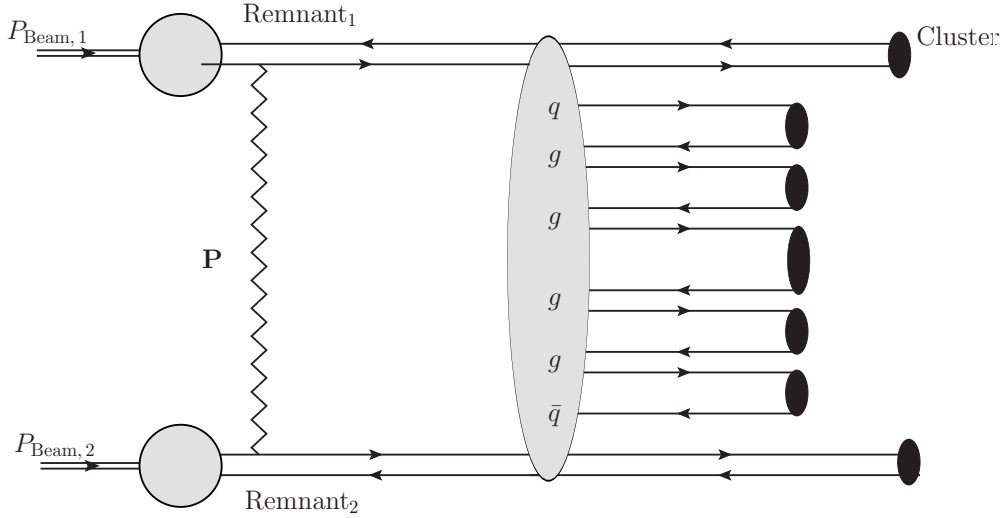


Figure 5.5.: Colour connections between the particles in the multiperipheral ladder and between the remnant and the hard scattering part of the event. A colour line is represented as an arrow towards the right and an anti-colour line is represented as an arrow towards the left. A colour line is connected to an anti-colour line such that clusters are formed from neighbouring particles in rapidity. The toy process is denoted by \mathbf{P} .

which are explicitly not considered in the tuning procedure particularly the rapidity gap analyses measured by CMS and ATLAS [40, 45].

5.3.1. General tuning procedure

Since we changed the soft part of the model for multiple parton interaction, we need to re-tune all parameters that affect this model directly. In Ref. [37] an energy dependent parameterisation for p_{\perp}^{\min} was adapted,

$$p_{\perp}^{\min}(s) = p_{\perp,0}^{\min} \left(\frac{\sqrt{s}}{E_0} \right)^b, \quad (5.40)$$

with $E_0 = 7$ TeV. The main parameters of the model therefore are:

- $p_{\perp,0}^{\min}$ parameter of the p_{\perp}^{\min} parameterisation of Eq. (5.40),
- b parameter of the p_{\perp}^{\min} parameterisation of Eq. (5.40),
- μ^2 inverse hadron radius squared used in the calculation of the overlap function, Eq. (4.4),
- p_{Reco} reconnection probability of the plain colour reconnection model [37],

- n_{Ladder} ladder multiplicity that influences the number of particles in one ladder.

We also decide to tune the probability for colour reconnection because we expect this parameter to have a significant effect on the clusters that originate from the ladders. Further we leave the remaining hadronisation parameters untouched which were tuned to data from LEP experiments [31]. According to Ref. [43] the tuning of 5 parameters with a 4-dimensional interpolation requires at least 126 runs and since an oversampling of at least a factor of 3 is advised we generate 500 runs. Every run consists of 500000 events with randomly selected parameter values in the ranges given in Tab. (5.1).

A subset of these 500 runs is then used 350 times to interpolate the generator response. For each of these run combinations the χ^2/N_{dof} value is calculated and real Monte Carlo runs were performed in order to check if the interpolation indeed predicted the right value of χ^2/N_{dof} . The parameter set that resulted in the smallest value of χ^2/N_{dof} was then used for further work.

5.3.2. Tuning to minimum bias data

Minimum bias is an experimental term that refers to a minimal possible trigger requirement necessary to include inelastic collisions. These minimum bias measurements include both, diffractive and non-diffractive processes. With the softMPI model Herwig should be able to describe inclusive minimum bias data completely. We tune the new model to data from the ATLAS collaboration at $\sqrt{s} = 900 \text{ GeV}$ and $\sqrt{s} = 7 \text{ TeV}$ [38]. For the tuning procedure we use eight different observables with equal weights:

- The Pseudorapidity distributions for $N_{\text{ch}} \geq 1$, $N_{\text{ch}} \geq 2$, $N_{\text{ch}} \geq 6$, $N_{\text{ch}} \geq 20$,
- The transverse momentum of charged particles for $N_{\text{ch}} \geq 1$, $N_{\text{ch}} \geq 2$, $N_{\text{ch}} \geq 6$,
- The average charged transverse momentum vs. number of charged particles for $N_{\text{ch}} \geq 1$.

In App. A the results of the tuning procedure for different run combinations are shown for 900 GeV and 7 TeV.

Except for the parameter b at 7 TeV all other parameters are distributed around one value, indicating that the used observables are very sensitive to the tuned parameters. A broader distribution means less sensitivity but a more flexible parameter choice. It is especially important to note that $p_{\perp,0}^{\text{min}}$ and b have approximately the same value for 900 GeV and 7 TeV, showing that the parameterisation of the $p_{\perp}^{\text{min}}(s)$ parameter from of Eq. (5.40) is sensible. The inverse proton radius μ^2 , which controls the matter distribution

inside the proton and the reconnection probability p_{Reco} seem to favor different values indicating an energy dependence of these parameters. The newly introduced parameter n_{Ladder} favours values around $n_{\text{Ladder}} \approx 0.7$ for $\sqrt{s} = 7$ TeV and values around $n_{\text{Ladder}} \approx 1.1$ for $\sqrt{s} = 900$ GeV. This seemingly energy dependence will be discussed later in Sec. 5.4.3.

The tuned parameters, their default values and the results of the tuning procedure are listed in Tab. 5.1. With the newly introduced softMPI model and the tuned parameters the description of all minimum bias observables improves significantly although we only tuned to a small subset of available observables. The results for the Monte Carlo runs with the tuned parameters for 900 GeV and 7 TeV are shown in Figs. 5.6 and 5.7. Here we only show the two most inclusive η distributions, the distribution for the charged particle p_{\perp} and the charged particle p_{\perp} versus the number of charged particles N_{ch} . It is especially noteworthy that the new model fits the charged particle p_{\perp} distribution almost perfectly in the range where we expect the new softMPI model to contribute significantly. Also the onset of the charged particle p_{\perp} versus the number of charged particles improves which is due to diffraction. The tail of this distribution seems to underestimate the p_{\perp} value but the tune results in an overall better description of the observables.

| | Default | Range | MB-900 | MB-7 |
|---|---------|-----------|----------|----------|
| p_{Reco} | 0.4276 | 0.0 – 1.0 | 0.647048 | 0.445557 |
| $p_{\perp,0}^{\text{min}} / \text{GeV}$ | 4.39 | 1.0 – 5.0 | 3.407673 | 3.145333 |
| μ^2 / GeV^2 | 2.30 | 0.0 – 2.0 | 1.548230 | 1.101560 |
| b | 0.366 | 0.0 – 2.0 | 0.444223 | 0.709107 |
| n_{Ladder} | none | 0.0 – 2.0 | 1.155612 | 0.700985 |

Table 5.1.: Parameter values and ranges used in the tuning of the new softMPI model. Shown are the tunes resulting in the smallest χ^2/N_{dof} value for 900 GeV and 7 TeV centre-of-mass energy \sqrt{s} .

5.4. Results

In this section we discuss the results when we apply our new model to other observables. This is an important cross check for the validity of the model. We will see that the model is not only able to describe the observables it was explicitly tuned to, but also manages to achieve good overall results in the whole range of minimum bias related analyses available.

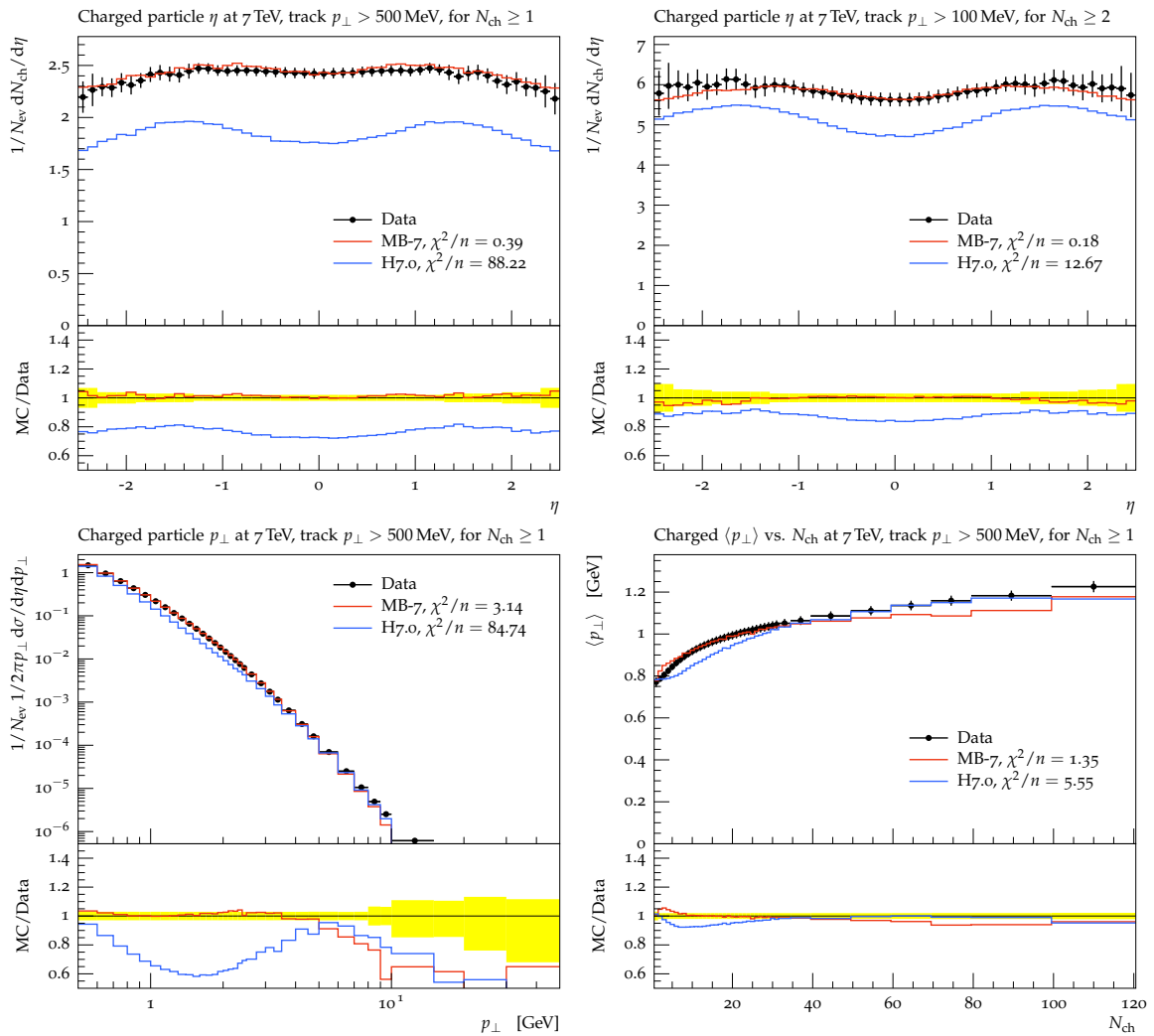


Figure 5.6.: Comparison of the default tune from Herwig 7.0 with the best tune (MB-7) for the new softMPI model to minimum-bias data from ATLAS [38] at $\sqrt{s} = 7$ TeV.

5.4.1. Rapidity gap analysis

The total cross section of hadronic collisions can be decomposed into two main components,

$$\sigma_{\text{tot}} = \sigma_{\text{el}} + \sigma_{\text{inel}} , \quad (5.41)$$

where σ_{el} is the elastic- and σ_{inel} is the inelastic-cross section. The elastic cross section describes proton scattering where the protons remain intact after the collision. The inelastic cross section σ_{inel} consists of all events where the proton gets destroyed. σ_{inel} can be separated into diffractive (D) and non-diffractive events (ND). The diffractive events

5. Multiperipheral particle production

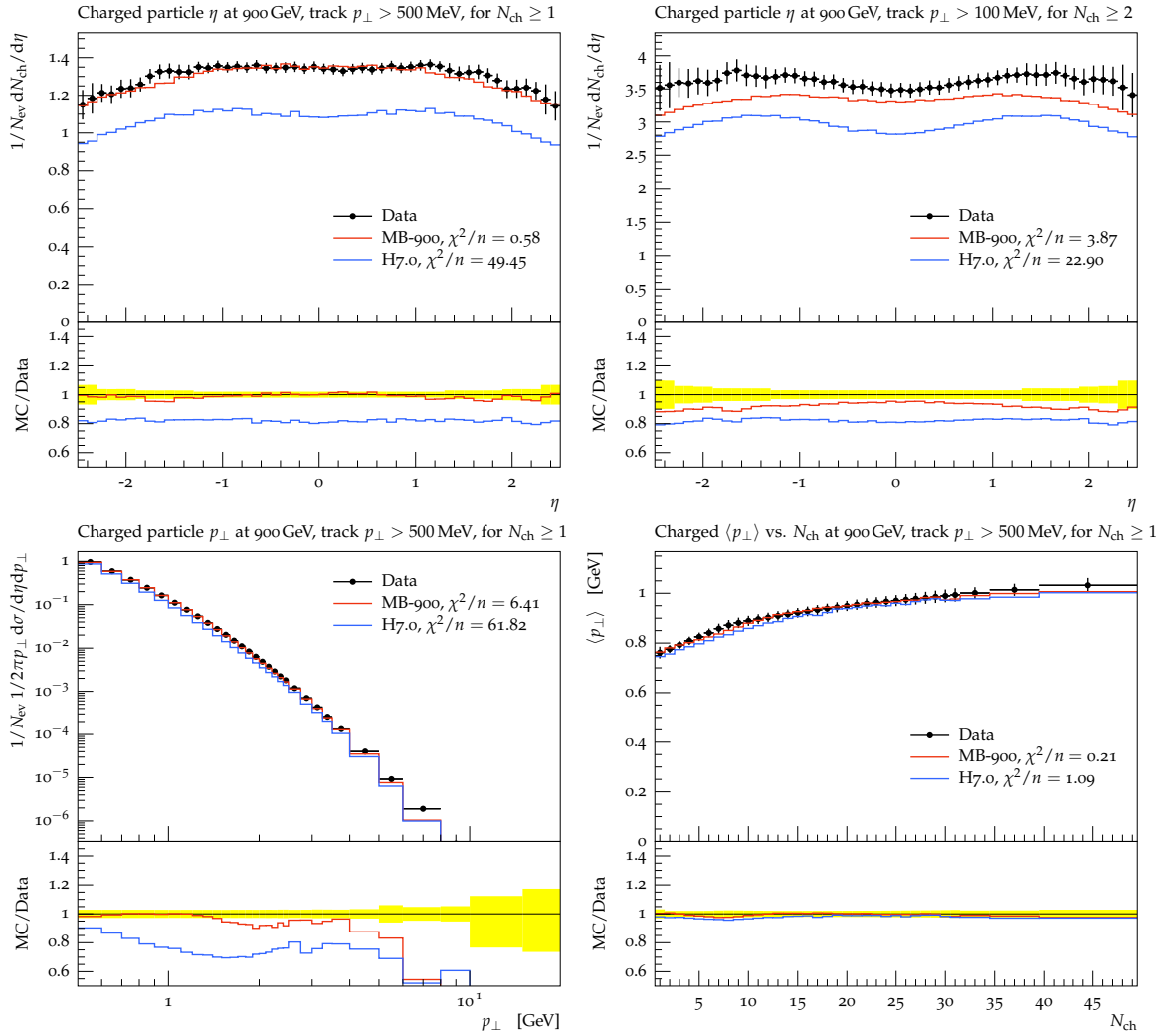


Figure 5.7.: Comparison of the default tune from Herwig 7.0 with the best tune (MB-900) for the new softMPI model to minimum-bias data from ATLAS [38] at $\sqrt{s} = 900$ GeV.

can be further separated into single-diffractive (SD) and double-diffractive processes (DD)

$$\sigma_{\text{inel}} = \sigma_{SD} + \sigma_{DD} + \sigma_{ND} . \quad (5.42)$$

In the detector diffractive processes are associated with colourless exchanges resulting in a large rapidity interval without any hadronic activity which is referred to as the *rapidity gap*. The rapidity gap is used to characterise diffractive events since the direct analysis of the dissociated systems is difficult and many of the final state particles are not within detector sensitivity.

In Refs. [40] and [45] the cross section with respect to the forward pseudorapidity gap $\Delta\eta^F$ is measured. $\Delta\eta^F$ is defined as the larger of two pseudorapidity regions in which no particles are produced. $\Delta\eta$ ranges from -4.9 to $+4.9$ at ATLAS and from -4.7 to $+4.7$ at CMS, which is restricted by the geometry of the detectors. All particles with $p_{\perp} > p_{\perp}^{\text{cut}}$ are analysed where p_{\perp}^{cut} is varied from 200 GeV to 800 GeV. This observable can be decomposed into a ND - and a SD/DD part of the cross section where small gap sizes are mainly dominated by ND contributions and for a small p_{\perp}^{cut} the large rapidity gap region is dominated by SD and DD events. The ND part is characterised by the experimental observation that the average rapidity difference between neighbouring particles is around 0.15 with larger rapidity gaps due to fluctuations in the hadronisation process. This leads to a cross section that decreases exponentially with larger rapidity gaps $\sigma_{ND} \sim \exp(-a\Delta\eta^F)$ where a is some unknown constant. The large rapidity gaps are due to the colourless exchange of diffractive events which gives rise to a constant cross section $\sigma_D \approx \text{const.}$

Together with the diffraction model from Ref. [39] Herwig 7 is able to describe the measurement of the rapidity gap cross section from ATLAS [40] and CMS [45] correctly (see Fig. 5.8). While the data from CMS is described very well, the simulation overestimates the data provided by ATLAS despite quite similar cuts. This might indicate some discrepancies between the two analyses but nevertheless the prediction of the new softMPI model is within acceptable range.

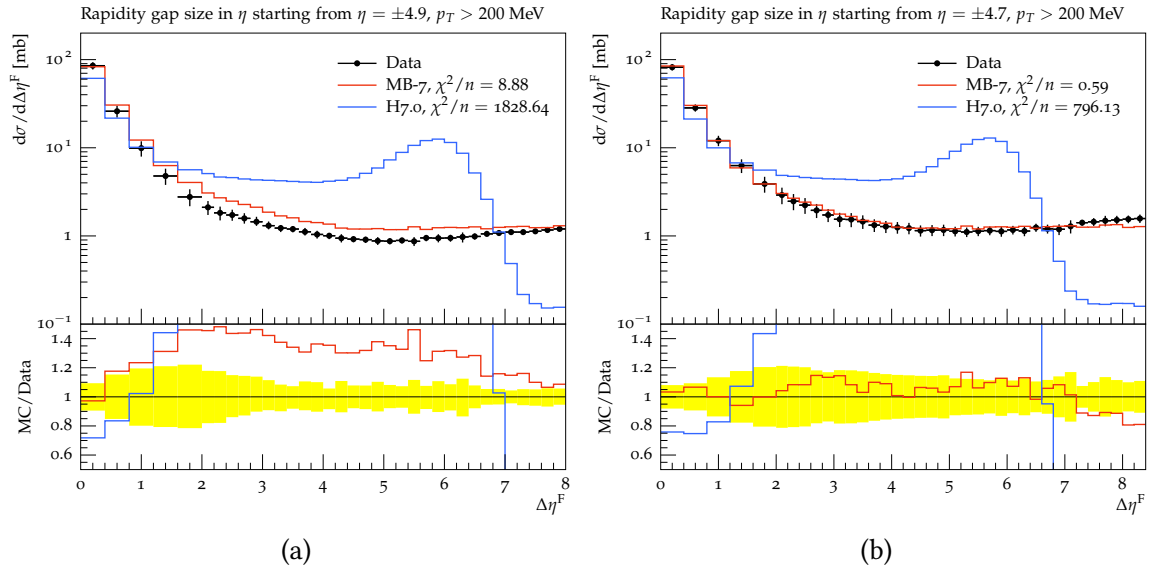


Figure 5.8.: Pseudo rapidity gap distribution for a low p_{\perp} cut from ATLAS [40] (a) and CMS [45] (b). Shown is the comparison between the old model from Herwig 7 and the 7 TeV minimum bias tune of the new softMPI model.

5.4.2. Analysis of non-single-diffractive events

The analysis presented in Ref. [46] is based on an event selection which is corrected according to the SD, DD and ND events predicted by PYTHIA 6 [47]. Therefore this analysis is automatically biased by these predictions. It is none the less useful to see how our new softMPI model with the MB-7 tune performs with respect to these observables.

Although we note significant improvement in the region of low multiplicity the new model fails to describe the data correctly (see Fig. 5.9). It is interesting to note that in Ref. [46] it was found that the event generators systematically underestimated the increase of the multiplicity distribution while our model (and also the old default model) overestimate it. The multiplicity distribution is mainly influenced by the mass distribution of the clusters. The higher the cluster mass, the more particles get produced from the cluster. We expect a change in the colour reconnection model to have significant impact on these distributions which will be presented in Ch. 6.

In Ref. [48] a similar analysis was performed in order to study the transverse momentum distributions of non-single-diffractive events using the same corrections according to the predictions by PYTHIA. The new model shows a significant improvement and seems to describe the data correctly except for the ultra low $p_{\perp} < 0.4$ GeV region (see Fig. 5.10).

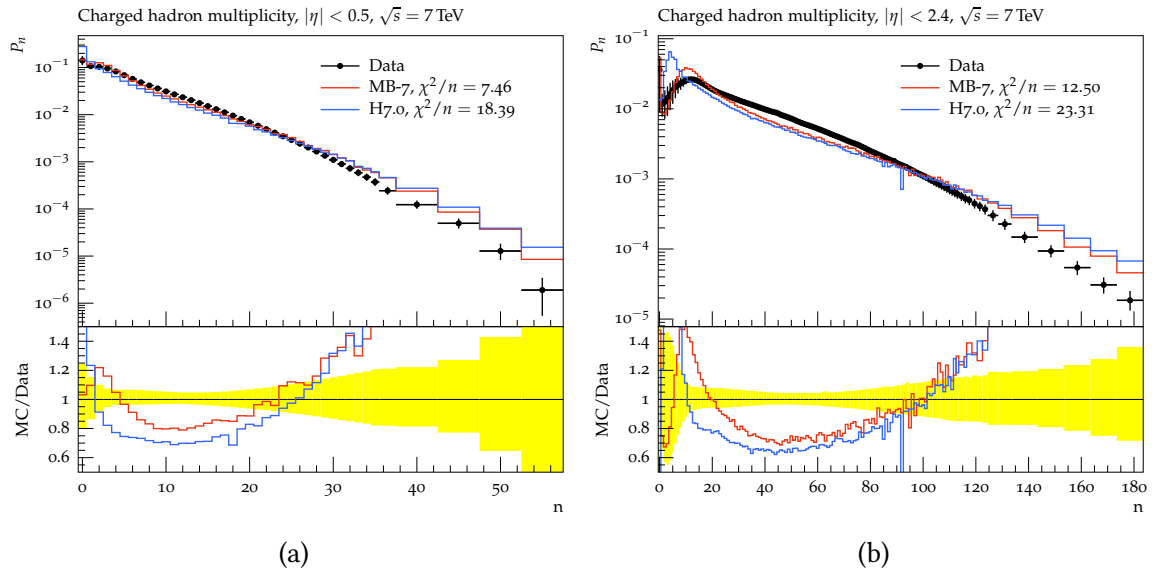


Figure 5.9.: Multiplicity distributions for the very central region $|\eta| < 0.5$ (a) and the most inclusive measurement by CMS [46] (b). MB-7 are all non-single-diffractive simulations while H7.0 uses the old model for multiple parton interactions and lacks a model for diffraction completely.

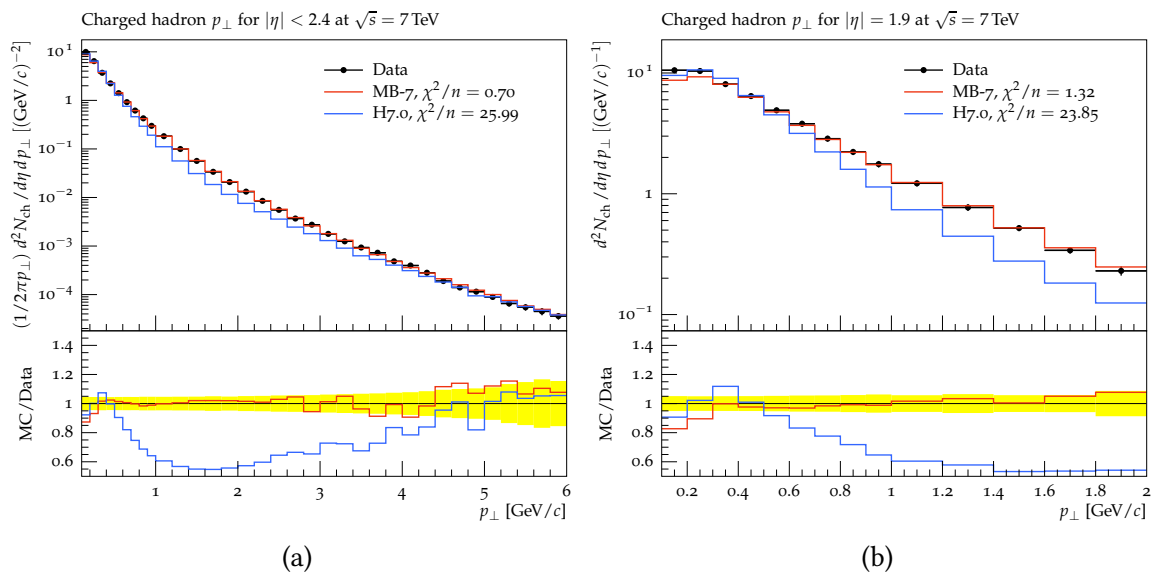


Figure 5.10.: p_{\perp} distributions for $|\eta| < 2.4$ (a) and $|\eta| = 1.9$ (b) measured by CMS [48]. MB-7 are all non-single-diffractive simulations while H7.0 uses the old model for multiple parton interactions and lacks a model for diffraction completely.

5.4.3. Extrapolation to 13 TeV

With the energy update of the LHC to 13 TeV in 2015 new sets of data are available. This data at the new energy frontier serves as an excellent cross check for our new model. In order to test the energy extrapolation we compare it to data provided by the ATLAS collaboration [49] at $\sqrt{s} = 13$ TeV. Although we used the same set of parameters as for $\sqrt{s} = 7$ TeV, the new model improves the description of the data compared to the old model significantly as shown in Fig. 5.11.

In Sec. 5.3.2 it was noted that we could not describe the data at 900 GeV and 7 TeV with the same set of parameters because the ladder multiplicity n_{Ladder} favours different values. A tuning procedure to 13 TeV resulted in almost identical values for the parameters as for 7 TeV. Especially the ladder multiplicity is with $n_{\text{Ladder}} \approx 0.65$ in the same range as for 7 TeV. It is interesting to note that with the tuned parameters we obtain for the average number of partons produced per ladder the following values,

$$\begin{aligned}
 \langle n_{900 \text{ GeV}} \rangle &= 10.7, \\
 \langle n_{7 \text{ TeV}} \rangle &= 9.5, \\
 \langle n_{13 \text{ TeV}} \rangle &= 10.2.
 \end{aligned}
 \tag{5.43}$$

Although the parameters seem to be energy dependent the produced number of particles per ladder is on average the same for all energies investigated.

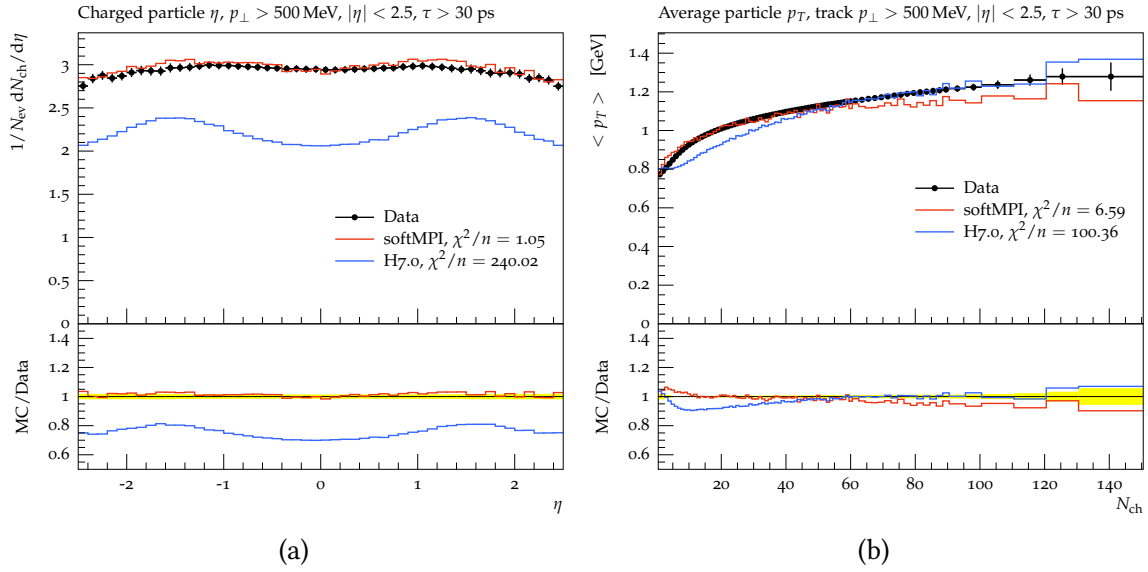


Figure 5.11.: Most inclusive η distribution for $p_{\perp} > 500$ MeV (a) and average p_{\perp} distribution for all particles with $p_{\perp} > 500$ MeV (b) measured by ATLAS [49] at $\sqrt{s} = 13$ TeV. The runs for softMPI were done with the tuned set of parameters for 7 TeV. H7.0 uses the old model for multiple parton interactions.

5.5. Conclusion

We have introduced a new model for soft multiple parton interactions inspired by multiperipheral particle production. In this region the soft emission of gluons is no longer described by an elastic two to two scattering, rather we use a more sophisticated model inspired by the ideas of Regge theory. The model is implemented as the production of ladders of n -particles that are ordered equally in rapidity. The parameters of the new soft part of the multiple parton interaction model in combination with the new n_{Ladder} parameter and the model for diffraction were tuned to minimum bias data at $\sqrt{s} = 900$ GeV and $\sqrt{s} = 7$ TeV. With the tuned parameters the new model improves the description of all minimum bias observables significantly. We also showed that the 7 TeV tune is able to describe 13 TeV data. The new soft model is able to describe the cross section in the low rapidity gap region $\sim e^{-\Delta\eta^F}$ correctly. Furthermore in non-single-diffractive event analyses, the model improves the description of multiplicity distributions and gives the correct description of the p_{\perp} distributions.

6. Colour reconnection

In order to describe the full structure of a particle scattering process additional soft effects that are not accessible by perturbation theory have to be considered. Such effects include hadronisation, multiple parton interactions and particle fragmentation. In general these non-perturbative effects are based on phenomenological considerations. The basis for the hadronisation model in Herwig 7 is the cluster model [23] (see Sec. 3.3) which forms colourless singlets from colour connected particles. The fragmentation of these clusters into hadrons depends on the invariant cluster mass and the flavour of the quarks inside the cluster. Colour connections between the partons in an event are determined by the $N_C \rightarrow \infty$ approximation which leads to a planar representation of quark lines [21]. Every parton is connected to another parton and gluons, carrying both colour and anti colour are connected to two other partons.

The goal of *colour reconnection* is to study whether different connection topologies, other than the predefined colour connection, are possible between the partons.

A good example for the effect of colour reconnections is the process

$$e^+e^- \rightarrow W^+W^- \rightarrow (q_1\bar{q}_2)(q_3\bar{q}_4), \quad (6.1)$$

which was extensively studied at LEP-2. Due to the small lifetime of the W -bosons the decay vertices of the two W 's are less than 0.1 fm apart from each other which leads to a large spacetime overlap of the decaying products. Therefore the hadronic systems are in contact which may lead to colour interchange between the different systems and one quark of the W^+ boson may hadronise together with the antiquark of the other W^- boson,

$$(q_1\bar{q}_2)(q_3\bar{q}_4) \rightarrow (q_1\bar{q}_4)(q_3\bar{q}_2). \quad (6.2)$$

This effect was first studied by Gustafson, Peterson and Zerwas [50] and non-perturbative models for colour reconnection were proposed by Sjöstrand and Khoze [51]. Hadronic collisions consist of a much more complicated structure than e^+e^- collisions. In a pp collision for example the hard scattering is accompanied by multiple parton interactions that all reside within the proton radius which leads to a significant increase in hadronic

activity. Models for colour reconnection have shown to be indispensable for describing LHC and Tevatron data. For example the distribution of mean transverse momentum $\langle p_{\perp} \rangle$ of charged particles over the number of charged particles N_{ch} , can only be described when colour reconnection effects are taken into account. In Fig. 6.1 this effect is shown with data from ATLAS [38]. If each interaction would be independent, $\langle p_{\perp} \rangle$ would be independent of N_{ch} . Colour reconnection reduces the multiplicity in the event while p_{\perp} remains the same and is shared among the produced hadrons which results in a rise of the $\langle p_{\perp} \rangle(N_{\text{ch}})$ distribution. In the context of our work we already implemented a new model for the soft part of the multiple parton interaction model and achieved good results in describing minimum bias and underlying event data. Due to the multiperipheral ladder structure we have more smaller clusters and expect the effects of colour reconnections to be less significant than in the old model for multiple parton interactions. Also in recent pp collision data from the LHC [52] an underestimation of Hyperons (Λ) was found in simulations done with PYTHIA which triggered the studies performed in Ref. [53]. A similar deficiency can be found in simulations by Herwig 7, which indicates that the production mechanism of strange quarks has to be reconsidered.

In this chapter we consider additional allowed colour reconnection topologies complementary to the implemented models in combination with the new model for softMPI (see Ch. 5) and investigate the effects on different observables.

In Sec. 6.1 we briefly summarise and explain the existing models for colour reconnection before we describe the implemented extensions in Sec. 6.2. In Sec. 6.3 we re-tune the parameters of the new softMPI model with the new parameters of the extended colour reconnection model to data from pp collisions and discuss the effects on baryon production. Finally, in Sec. 6.4 we present our results and give a quick summary.

6.1. Colour reconnection models in Herwig 7

In Herwig 7 colour reconnection is implemented directly before the cluster fission (see Sec. 3.3.2) takes place. Colour reconnection allows to rearrange clusters in a way that would not be allowed by the given colour connections of the original topology and results therefore in a different cluster configuration. This is shown in Fig. 6.2 for an event with three clusters. The properties of a cluster are defined by the invariant cluster mass, which is given by

$$M^2 = m_1^2 + m_2^2 + 2(E_1 E_2 - \mathbf{p}_1 \cdot \mathbf{p}_2), \quad (6.3)$$

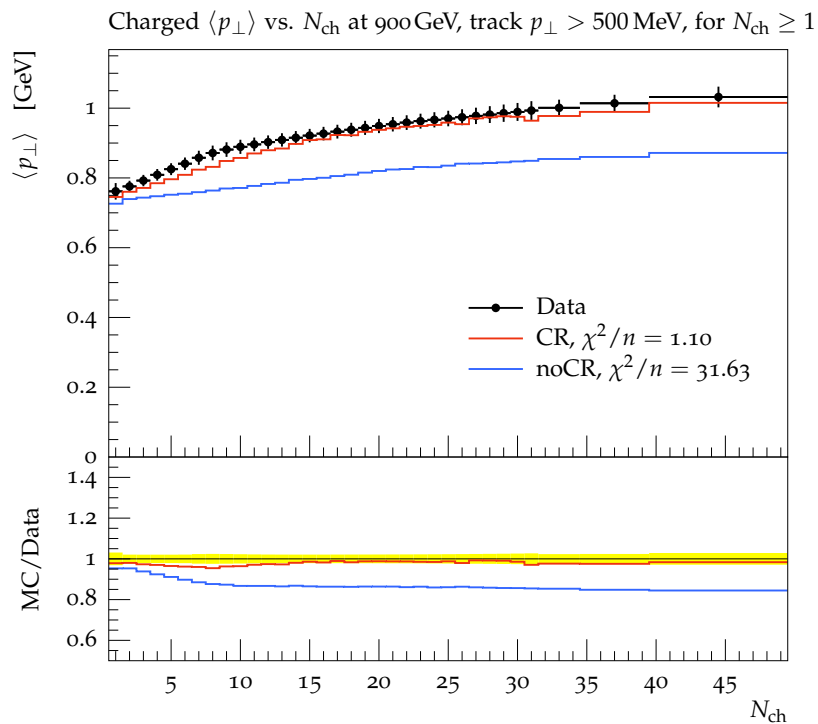


Figure 6.1.: Comparison of Herwig 7 with and without colour reconnection (CR) to the $\langle p_{\perp} \rangle(N_{\text{ch}})$ distribution measured by ATLAS [38] at 900 GeV for all particles with $p_{\perp} > 500$ MeV.

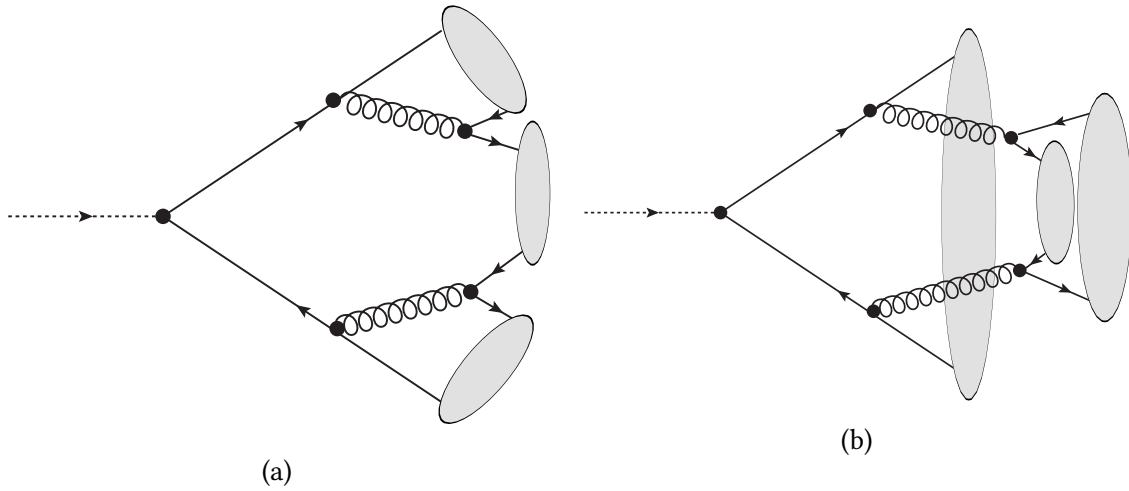


Figure 6.2.: Shown are two possible cluster configuration of simple event with three clusters. (a) Original configuration. (b) Configuration after colour reconnection.

where m_i are the masses of the constituents, E_i are the energies and \mathbf{p}_i are the momenta. The fission and the decay of the clusters directly depend on the invariant mass of the clusters which therefore directly influences the particle multiplicity.

Two algorithms for colour reconnection are implemented in Herwig 7, the *plain* colour reconnection and the *statistical* colour reconnection [37]. Both algorithms try to find configurations of clusters that would reduce the sum of invariant cluster masses, which is referred to as the *colour length*

$$\lambda = \sum_{i=1}^{N_{cl}} M_i^2 . \quad (6.4)$$

6.1.1. Plain colour reconnection

This algorithm is used by the default settings of Herwig 7. One quark is randomly picked from the list of clusters and the cluster it contains, A , is compared to all other clusters in that list. For every cluster the invariant masses of the original cluster configuration $M_A + M_B$ and the masses of the possible new clusters $M_C + M_D$ are calculated. The cluster configuration that resulted in the lowest sum of cluster masses $M_C + M_D$ is accepted for reconnection with a probability p_{Reco} . If the reconnection is accepted the clusters A and B are replaced by the new configuration of clusters C and D . This algorithm works out clusters with smaller invariant masses than the original configuration and therefore replaces heavy clusters with lighter ones resulting in a shift of the mass distribution towards lighter clusters.

6.1.2. Statistical colour reconnection

In the common approaches colour reconnection can be seen as a minimisation problem of the colour length λ . In order to find the global minimum of λ all possible combinations of clusters have to be considered. In hadronic pp collisions a brute force approach is an impossible venture due to the large amount of clusters originating from the hard process and multiple parton interactions. A more sophisticated approach was implemented in Ref. [37]. The statistical Colour Reconnection algorithm aims to find a configuration of clusters that results in a preferably low value of λ . For this a simulated annealing algorithm [54] is applied to find a good approximation of the global minima. The algorithm selects random pairs of clusters and accepts the reconnection if the new configuration lowers λ . If the reconnection would raise λ it is accepted with a probability $\propto \exp(-\frac{\lambda_2 - \lambda_1}{T})$, where T is the control parameter of the annealing algorithm that allows to accept steps that would raise λ . With the possibility to accept reconnections that would raise λ , the algorithm is able to escape local minima and converges to a configuration with a minimum value of λ . In Ref. [37] it was shown that in order to describe the data the algorithm prefers a quick cooling that does not result in the global minimum.

6.1.3. Effect of colour reconnection on the new softMPI model

It is interesting to see how colour reconnection changes the colour connections from the new softMPI model. If we recall Ch. 5, the gluons emitted in one ladder are ordered in rapidity and connected to the nearest neighbours. Since the multiperipheral ladder model creates more lighter clusters we expect the effects of colour reconnection on this model to be less significant than on the old model for multiple parton interactions.

In Fig. 6.3 we show the invariant mass distribution of clusters before and after colour reconnection for the old multiple parton interaction model and for the new softMPI model. The effect of colour reconnection on the new softMPI is much less significant than on the old model. The peak of the distribution is already at relatively low cluster masses $O(1 - 3 \text{ GeV})$ which can be seen in Fig. 6.4. This is due to the fact that within the ladder mainly clusters with low invariant masses are getting produced.

6.2. Extensions to colour reconnection

The only constraint upon forming a cluster is that the cluster has to be a colourless singlet under $SU(3)_C$. In $SU(3)_C$ a coloured quark is represented as a triplet (3) and an anticoloured antiquark is represented as an antitriplet ($\bar{3}$). For the discussion it is useful to

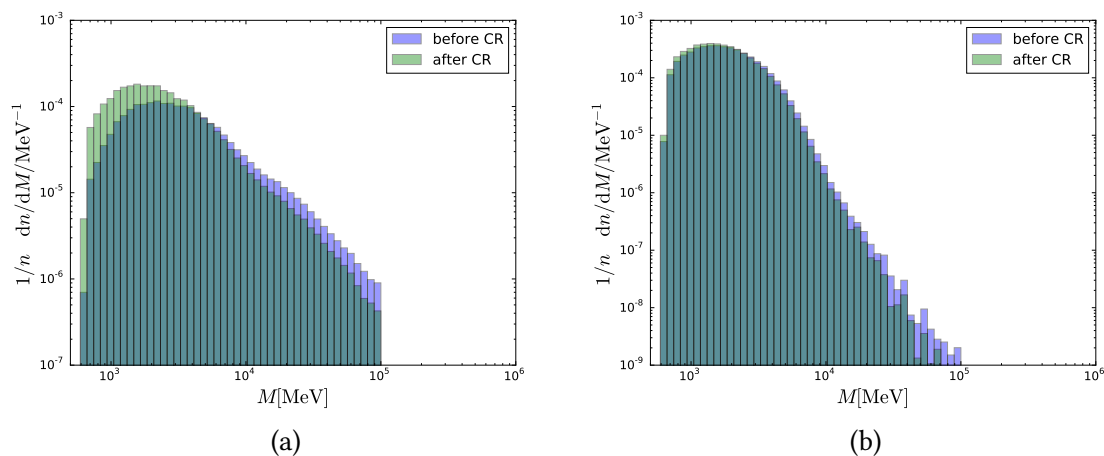


Figure 6.3.: Invariant mass distributions of clusters before and after colour reconnection for the old (a) and the new model for multiple parton interactions (b). The simulations for the new softMPI model were done without diffractive events.

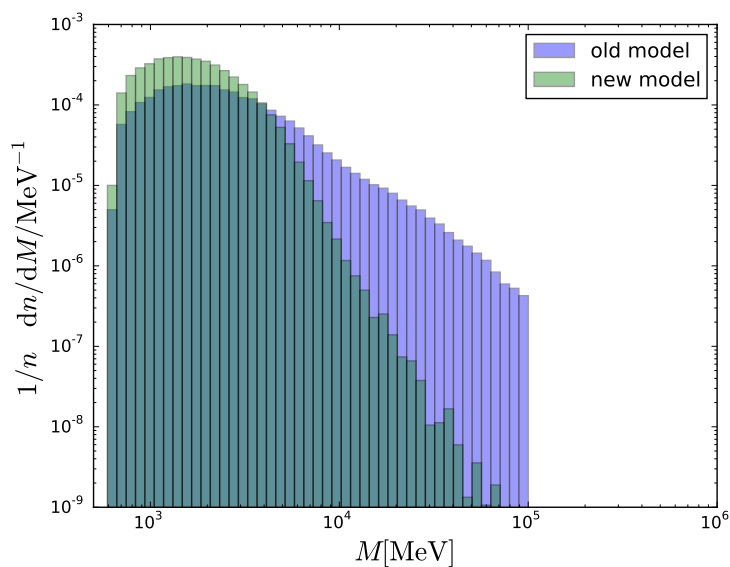


Figure 6.4.: Comparison of the invariant mass distribution between the two models for multiple parton interactions after colour reconnection.

note that two triplets can be represented as an anti-triplet and two anti-triplets can be represented as a triplet,

$$\begin{aligned} 3 \otimes 3 &= 6 \oplus \bar{3}, \\ \bar{3} \otimes \bar{3} &= 6 \oplus 3. \end{aligned} \tag{6.5}$$

The final cluster is a combination of these coloured quarks where only combinations are allowed that result in a singlet representation. For the extension to the colour reconnection model considered in this work we consider the following allowed configurations based on the $SU(3)_C$ structure of QCD. We begin with the normal cluster configuration which will be referred to as *mesonic cluster*. This cluster consists of a quark and an anti-quark. In $SU(3)_C$ a 3 and a $\bar{3}$ can be in an octet or a singlet state,

$$3 \otimes \bar{3} = 8 \oplus 1. \tag{6.6}$$

It is therefore possible for a quark-antiquark pair to form a singlet. If one considers the full $SU(3)_C$ the probability of a quark and an antiquark having the correct colours to form a singlet would be 1/9. Next we consider another cluster configuration which we will refer to as *baryonic cluster*. A baryonic cluster consists of three quarks or three antiquarks where the possible representations are,

$$\begin{aligned} 3 \otimes 3 \otimes 3 &= 10 \oplus 8 \oplus 8 \oplus 1, \\ \bar{3} \otimes \bar{3} \otimes \bar{3} &= 10 \oplus 8 \oplus 8 \oplus 1. \end{aligned} \tag{6.7}$$

The probability for three quarks to have the correct colour in order to form a singlet would be 1/27 under full $SU(3)_C$.

As explained before the colour reconnection models in Herwig 7 are implemented in such a way that a rearrangement of clusters is considered if it results in a lower sum of the invariant cluster masses λ . For baryonic clusters such a condition for reconnection is no longer reasonable. As an alternative we consider a reconnection mechanism based on the rapidity, y .

The rapidity y is defined as

$$y = \frac{1}{2} \ln \left(\frac{E + p_z}{E - p_z} \right), \tag{6.8}$$

and is usually calculated with respect to the z-axis. If a particle has little momentum along the defined axis, the rapidity goes towards zero and if a particle moves basically in the same direction as the axis, the rapidity goes to infinity. This way the rapidity indicates

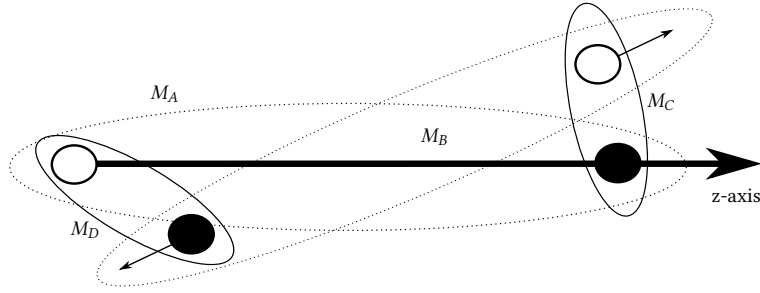


Figure 6.5.: Representation of rapidity based colour reconnection where the quark axis of one cluster is defined as the z -axis in respect to which the rapidities of the constituents from the possible reconnection candidate are calculated. M_A and M_B are the invariant masses of the original clusters. M_C and M_D are the invariant masses of the clusters after reconnection.

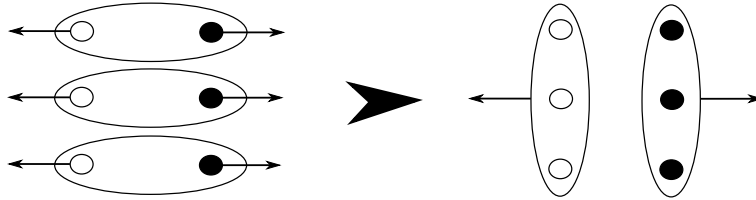


Figure 6.6.: Representation of clusters that might lead to baryonic reconnection. The black arrows indicate the direction of the quarks. A reconnection is considered if all quarks moving in the same direction and all antiquarks moving in the same direction.

in which direction a particle is moving relative to a certain axis which will be useful in deciding whether two particles are moving in the same direction or not. A reconnection algorithm based on the rapidity of the particles will consider clusters for reconnection if the constituents are flying in the same direction. If we recall the squared invariant mass of a cluster from Eq. (6.3) we see that the invariant mass of a cluster containing two quarks flying in the same direction will be lower than a cluster where the quarks fly in opposite directions. A reconnection will therefore directly reduce the number of particles that are produced due to cluster fission. A visualisation of the rapidity based colour reconnection is depicted in Fig. 6.5. Here the z -axis is defined as the quark axis of the cluster. A simplified sketch for baryonic reconnection is shown in Fig. 6.6. Here we consider reconnection if the quarks and the anti-quarks are flying in the same direction. A reconnection of this kind produces two baryonic clusters.

6.2.1. Algorithm

The starting point for the new rapidity based model is the predefined colour configuration that emerges once all perturbative evolution by the parton shower has finished and the remaining gluons are split non-perturbatively into quark anti-quark pairs. In the next step a list of clusters is created from all colour connected quarks and anti-quarks. The colour reconnection algorithm then allows to change this predefined configuration of clusters. The final algorithm for rapidity based colour reconnection consists of the following steps:

We shuffle the list of clusters in order to prevent the bias that comes from the order in which we consider the clusters for reconnection. We pick a cluster from that list and boost into the rest-frame of that cluster. The quark and the anti-quark in that cluster are now flying back to back and we define the direction of the anti-quark as the positive direction of the quark axis. In the next step we loop over all remaining clusters and calculate the rapidity of the cluster constituents with respect to the quark axis of cluster A in the rest-frame of this cluster. Depending on the calculated rapidities of the constituents of cluster B , the cluster B falls into one of two categories:

$$\text{Mesonic: } y(q_B) > 0 > y(\bar{q}_B) .$$

$$\text{Baryonic: } y(\bar{q}_B) > 0 > y(q_B) .$$

If the rapidities of the constituents of cluster B fall into none of the categories listed above the cluster is not considered for reconnection. In the next step the category and the sum of the absolute values is saved $|y(q_B)| + |y(\bar{q}_B)|$ for the clusters with the two largest sums. If the cluster with the largest sum has the label *mesonic* then accept the reconnection with a probability given by the parameter p_{Reco} and if the clusters with the two largest sums have the label *baryonic* then consider them for baryonic reconnection with probability $p_{\text{RecoBaryonic}}$. These two reconnection probabilities are the parameters of the model and are tuned to data in the next section. If two baryonic clusters are formed, the clusters are removed from the list and not considered for further reconnection. This removal of clusters might bias the colour reconnection algorithm since it strongly depends on the order of clusters.

6.3. Tuning

In the e^+e^- environment we expect little changes with the new colour reconnection model due to the missing hadronic activity one faces at pp collisions. The new colour reconnection model doesn't change the colour structure significantly which is already well defined

by the parton shower. This was confirmed by comparing Herwig 7 with the old and with the new model for colour reconnection to a wide range of experimental data from LEP. In Fig. 6.7 we show an example of the effect of the new model compared with the old model for colour reconnection. We conclude that the description of the data is of the same quality and even improves the description in some cases. We keep the hadronisation parameters that were tuned to LEP data (see Ref. [31]) at their default values. In the next step we tune to data from hadron colliders where we follow a similar tuning procedure as presented in Sec. 5.3.1.

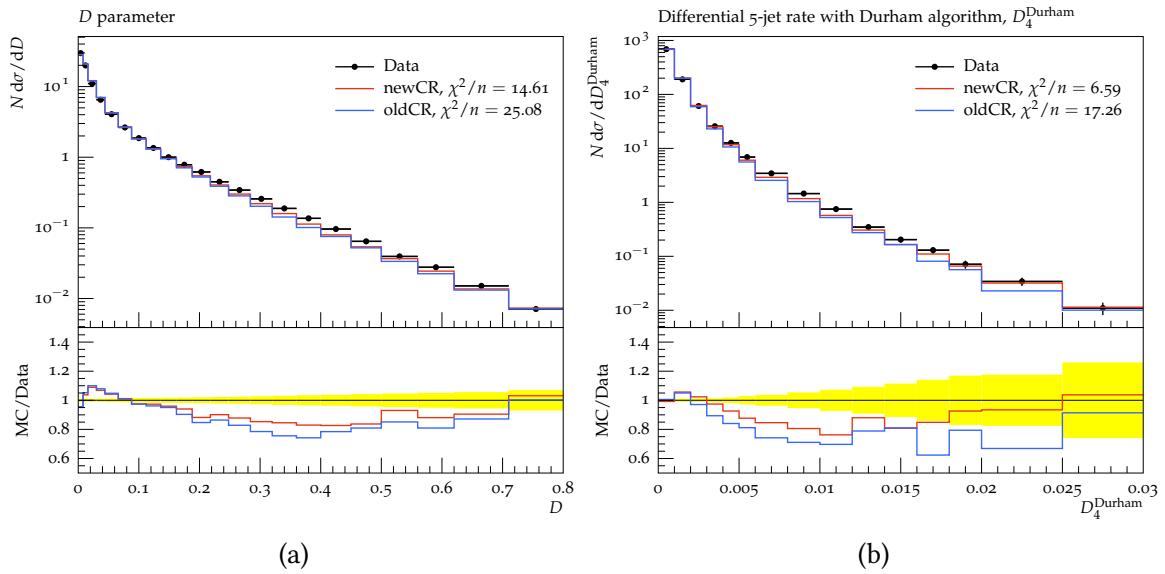


Figure 6.7.: Comparison between the new and the old colour reconnection model. Shown are two exemplary measurements from the DELPHI detector at LEP [55]. The value for $p_{\text{RecoBaryonic}}$ was set to 0.5.

6.3.1. Tuning to hadron colliders

The tuning of the new model for colour reconnection in combination with the model for the new softMPI consists of 6 main parameters, 5 of which were already explained in Sec. 5.3. The only new parameter of the model is the reconnection probability for baryonic clusters $p_{\text{RecoBaryonic}}$. In Fig. 6.8 we can see the influence of the new model for different values of $p_{\text{RecoBaryonic}}$ on the non-single-diffractive observables discussed in Sec. 5.4.2, where we used the parameters of Tab. 5.1. We already achieve a very good description of the data when applying the new model for colour reconnection. As expected the new reconnection model influences the hadronic multiplicities for large n significantly.

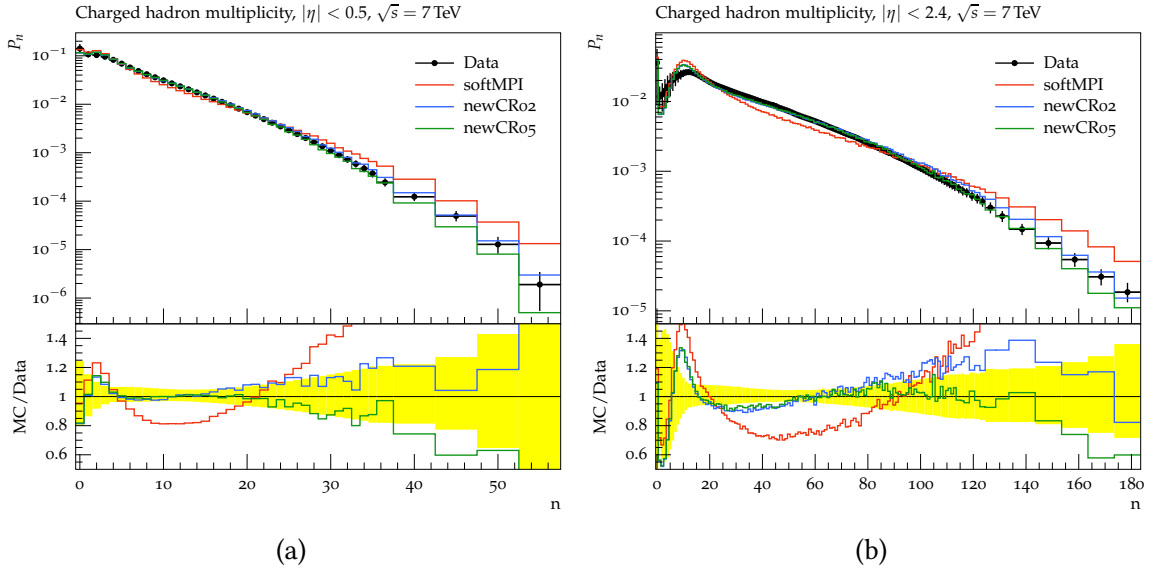


Figure 6.8.: Charged hadron multiplicities for different pseudo rapidity regions. Only non-single-diffractive events were simulated. The run for softMPI were performed with the new model for soft multiple parton interactions in combination with double diffractive events. The runs newCR02 and newCR05 were performed with the new softMPI model in combination with the new model for colour reconnection where we used 0.2 and 0.5 for the baryonic reconnection probability $p_{\text{RecoBaryonic}}$.

For the tuning we follow an iterative tuning procedure. We tune the two parameters of the new model to observables which are especially sensible to the effects of colour reconnection, the charged hadron multiplicity distributions and the $\langle p_{\perp} \rangle(N_{\text{ch}})$ distribution of Ref. [46] for all non-single-diffractive events.

We fix the parameters of p_{Reco} and $p_{\text{RecoBaryonic}}$ to the best values we get from the tuning and proceed to tune the other parameters of the model to the same minimum bias observables from Sec. 5.3. The results of this tune are shown for the most sensible observables in Figs. 6.9 and 6.10 where we compare the softMPI model in combination with the new and the old model for colour reconnection with the old MPI model of Herwig 7. Small differences can be seen in Fig. 6.9a. The new colour reconnection model gives the desired rise of the transverse momentum with respect to the number of charged particles. In Fig. 6.9b the new model gives a good description of the data between $N_{\text{ch}} = 25$ and $N_{\text{ch}} = 120$. For higher N_{ch} the distribution diverges from the data but this can be seen as missing statistics in the high N_{ch} region. For $N_{\text{ch}} < 25$ on the other hand, although the new model reduces the p_{\perp} per number of charged particles, it still is too large by a factor of ≈ 0.2 . If we compare this region to the corresponding region in Fig. 6.9a we note a

similar behaviour but not as significant. We conclude that ultra soft particles that are not included for $p_{\perp} > 500$ MeV carry too much transverse momentum on average.

In Fig. 6.10a we show the charged multiplicity as a function of the pseudorapidity η for $p_{\perp} > 100$ MeV and $N_{\text{ch}} \geq 20$. The new model improves the description in the central pseudo-rapidity region. In Fig. 6.10b we show the charged multiplicity distribution for $N_{\text{ch}} \geq 20$ and $p_{\perp} > 100$ MeV. We note the differences in the tail of the multiplicity distribution which is due the effect of the possibility for baryonic colour reconnection that reduces the multiplicities. The new model still overestimates the tail but performs significantly better than softMPI in combination with the old model for colour reconnection and the old model for multiple parton interactions of Herwig 7.

The model achieves very good results for the tuned observables and also for all other observables provided by ATLAS [38], which are not considered in the tuning procedure. With the additional possibility of having cluster reconnections that result in baryonic cluster we are able to describe the tails of the multiplicity distributions correctly. We also note slight improvements in the $\langle p_{\perp} \rangle(N_{\text{ch}})$ distribution.

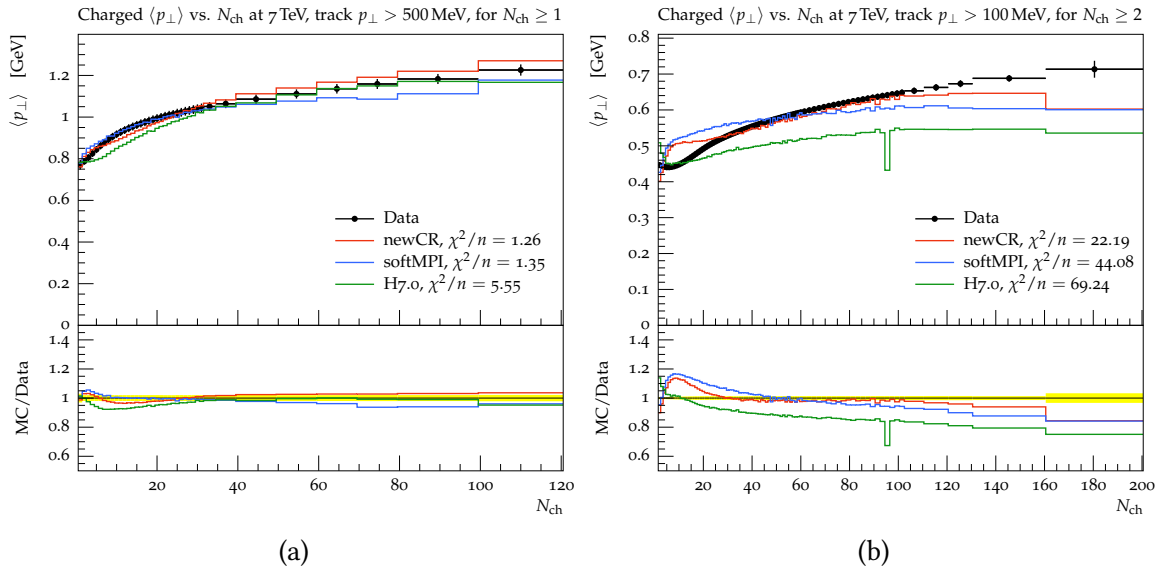


Figure 6.9.: Measurement of the average p_{\perp} as a function of multiplicity for two different cuts for p_{\perp} and $N_{\text{ch}} \geq 1$. (a) $p_{\perp} > 500$ MeV and $N_{\text{ch}} \geq 1$. (b) $p_{\perp} > 100$ MeV and $N_{\text{ch}} \geq 2$. The measurement was performed by the ATLAS collaboration [38].

The values of the tuned parameters in comparison with the tune presented in Sec. 5.3 are listed in Tab. 6.1. The baryonic reconnection probability seems to be quite high with a value of 0.45, but seems reasonable if we consider that the case of baryonic reconnection does not happen often. The other parameters are in the same region as the previous tune

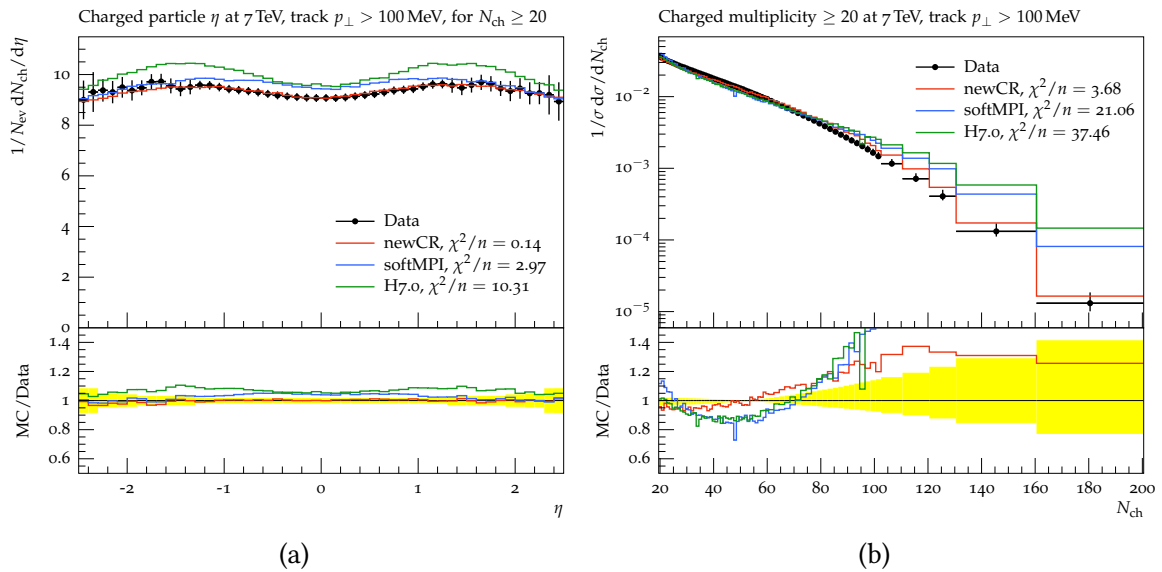


Figure 6.10.: Charged multiplicity as a function of pseudo-rapidity η for $p_{\perp} > 100$ MeV and $N_{\text{ch}} > 20$ (a), multiplicity distribution for $p_{\perp} > 100$ MeV and $N_{\text{ch}} \geq 20$. newCR is the softMPI model in combination with the new model for colour reconnection.

which indicates that the new model for colour reconnection is a reasonable extension to the softMPI model.

| | Default | Range | old CR | new CR |
|---------------------------------------|---------|-----------|--------|--------|
| p_{Reco} | 0.4276 | 0.0 – 1.0 | 0.4455 | 0.5535 |
| $p_{\text{RecoBaryonic}}$ | none | 0.0 – 1.0 | none | 0.4935 |
| $p_{\perp,0}^{\text{min}}/\text{GeV}$ | 4.39 | 1.0 – 5.0 | 3.1453 | 3.084 |
| μ^2/GeV^2 | 2.30 | 0.0 – 2.0 | 1.1015 | 1.163 |
| b | 0.366 | 0.0 – 2.0 | 0.7091 | 0.7772 |
| n_{Ladder} | none | 0.0 – 2.0 | 0.7009 | 0.7336 |

Table 6.1.: Parameter values and ranges used in the tuning of the softMPI model in combination with the new model for colour reconnection. Shown are the tunes resulting in the smallest χ^2/N_{dof} value for 7 TeV centre-of-mass energy \sqrt{s} .

6.4. Results

We tuned the two parameters of the new model to sensible observables for colour reconnection. We fixed these two parameters to their best value and re-tuned the parameters of the softMPI model to minimum bias data which results in an overall good description of

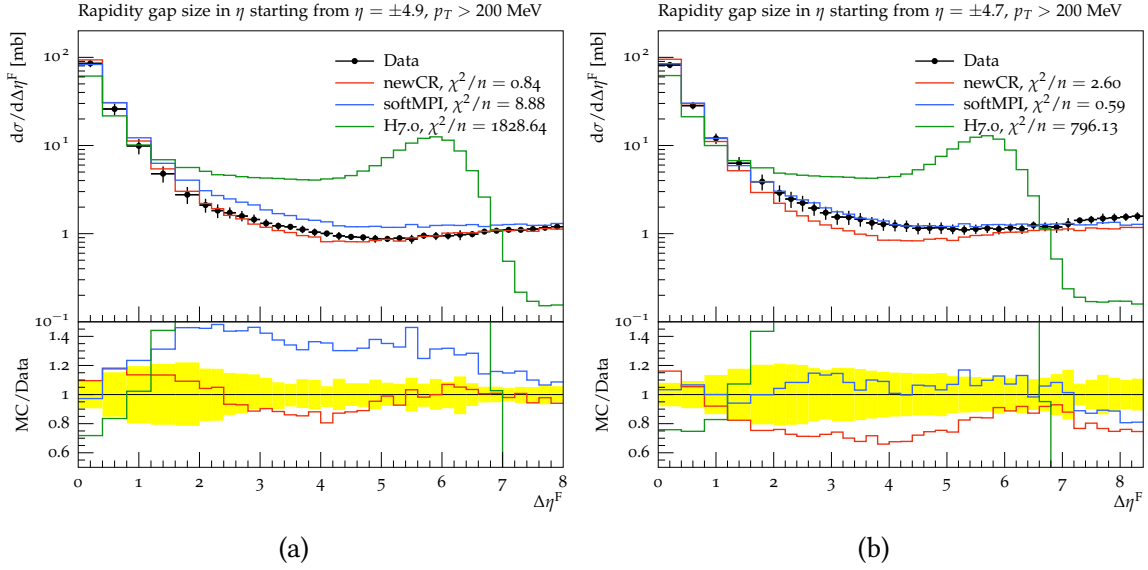


Figure 6.11.: Pseudo rapidity gap distribution for a low p_\perp cut from ATLAS [40] (a) and CMS [45] (b). Shown is the comparison between the softMPI model in combination with the new model for colour reconnection and the old model from Herwig 7.

the considered observables. Next we compare the new model with the tuned parameter values to other important observables as in Sec. 5.4.

6.4.1. Rapidity gap analysis

In Fig. 6.11 we show the rapidity gap distributions with the new model for colour reconnection. While in Fig. 6.11a the data is almost perfectly described by the new model the data in Fig. 6.11b is underestimated in the mid-range of the $\Delta\eta^F$ region for low p_\perp cutoffs. Now the measurement by ATLAS is better described than the measurement by CMS but the quality of description is quite high for both observables. The new model reduces the amount of events in the large $\Delta\eta^F$ region which is more in align with the property of the soft model for multi parton interactions that the contribution from non-diffractive events should be proportional to $e^{-\Delta\eta^F}$. We also note that the contribution in the large $\Delta\eta^F$ region for the softMPI model is due to the old colour reconnection model preferring cluster combinations that may result in a smaller invariant mass but create large gaps between the clusters which should only come from diffractive events.

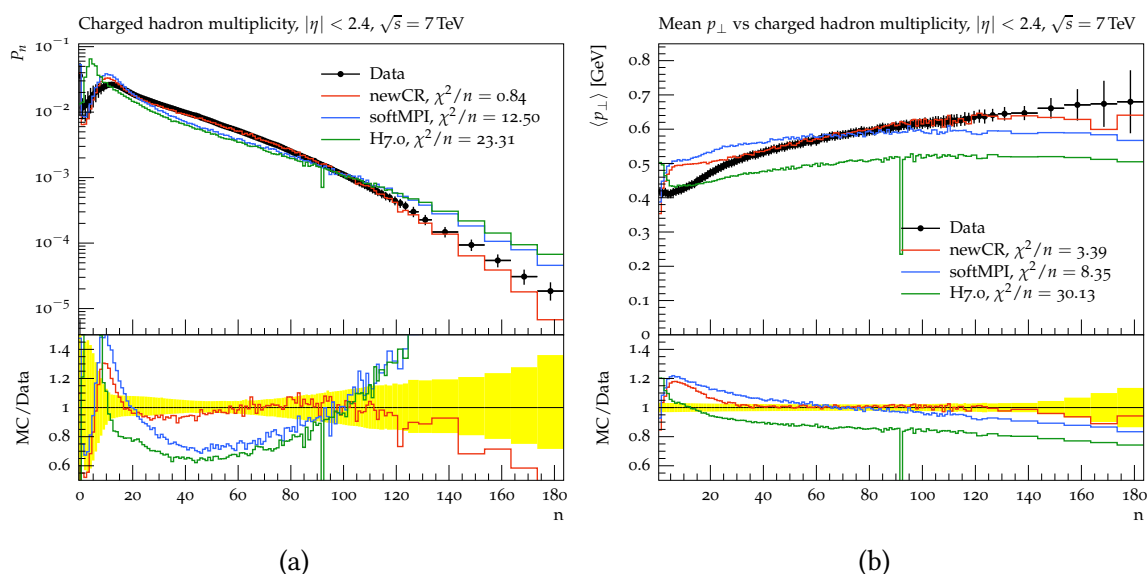


Figure 6.12.: Multiplicity distribution for the most inclusive measurement by CMS (a). Average p_\perp as a function of hadron multiplicity (b). The runs newCR and softMPI are non-single-diffractive simulations while H7.0 uses the old model for multiple parton interactions and lacks a model for diffraction completely.

6.4.2. Analysis of non-single-diffractive events

In Fig. 6.12a we see the expected fall off for high multiplicities. In combination with the new model for colour reconnection the softMPI model is able to describe the region $20 < n < 120$ fairly well compared to the model with the old colour reconnection. For $n > 120$ the model underestimates the data but is still within error bars. For Fig. 6.12b the same behaviour as for Fig. 6.9b is observed. The rise of p_\perp with number of charged particles is better described for non-single-diffractive events. Especially the new model agrees with the data for $n > 20$ and seems necessary to describe the rise of p_\perp with number of particles.

6.4.3. Baryon ratios

In Fig. 6.13a we see the effect of the new colour reconnection model on the transverse momentum distribution of Λ baryons. The new model as well as the old model underestimate the production of Λ baryons in all p_\perp regions significantly. The new model for colour reconnection increases the amount of baryons produced in the central p_\perp region but the effect is still not large enough. Especially the number of Λ baryons in the low p_\perp region is off by a large factor. This underestimation is not only a property of Λ baryons, also other hadrons containing strangeness are underestimated systematically as shown

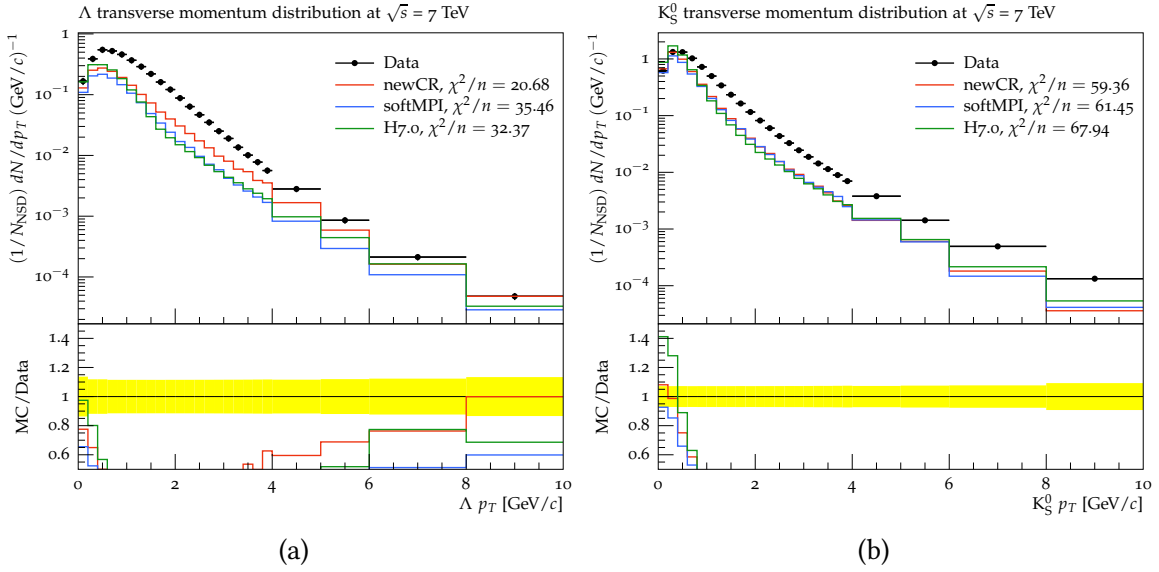


Figure 6.13.: Multiplicity distributions for the very central region $|\eta| < 0.5$ (a) and the most inclusive measurement by CMS [46] (b). MB-7 are all non-single-diffractive simulations while H7.0 uses the old model for multiple parton interactions and lacks a model for diffraction completely.

in Fig. 6.13b for the case of Kaons. This was also pointed out in Ref. [56]. The ratio Λ/K_s increases in the low p_\perp region but is still well below the data. Here we just point out that the new model gives a lever on the rate of baryons and mesons. A systematic retuning of parameters responsible for strangeness production might lead to a better description of these observables.

6.5. Conclusion

We introduced additional allowed possibilities for colour reconnection based on the $SU(3)_C$ structure of QCD in Herwig 7. The tuning to sensible observables for colour reconnection and minimum bias data resulted in an improved description of all considered observables. We especially found that the possibility of baryonic reconnection reduces the multiplicities in the tail of the number of charged particle distributions significantly which is necessary to describe non-single-diffractive analyses. The effects in terms of reduction of invariant cluster mass is quite low for the softMPI model since the majority of clusters in the ladder consists of quarks which are already close in rapidity. The description of the rapidity gap analysis improves due to the new colour reconnection model because it reduces the contribution from events with large $\Delta\eta$.

The description of hadrons containing strange quarks remains an ongoing construction site. The new colour reconnection model gives a lever on the production of hadrons but neither Λ nor K multiplicities are described satisfactorily. This might indicate that the production mechanism for strange baryons and mesons has to be reconsidered which could be done during gluon splitting, cluster fission and cluster decay. Also colour reconnection models which depend on the flavours of the constituents would be possible.

7. Summary and outlook

The aim of this work was to implement a new model for soft multiple parton interactions in Herwig 7. The model is based on multiperipheral particle production where one soft interaction produces a ladder of particles that are ordered in rapidity. It was shown that the invariant mass distribution of the clusters coming from that ladder already peaks at low masses of the order $O(\text{GeV})$ which means that the property of preconfinement is already fairly well satisfied.

In combination with diffraction the parameters of the new model for soft interactions were tuned to minimum bias data. With these new models Herwig 7 is for the first time able to describe minimum bias analyses completely. It was further shown that important observables such as the rapidity gap are now well described. It is possible to extrapolate the new model to 13 TeV and get very good results with a similar set of parameters as for 7 TeV. The new model showed some deviations when compared to non-single-diffractive analyses of charged hadron multiplicities. This issue is tackled in form of a new model for colour reconnection which is based on a rapidity picture rather than a direct comparison of invariant cluster masses. We introduced additional reconnection topologies like baryonic cluster formation and a re-tune of the model for multiple parton interactions in combination with the new model for colour reconnection was performed. It was shown that a combination with the new model for soft multiple parton interactions results in a better description of data and the deviation of charged hadron multiplicities is resolved. Also other important observables from minimum bias analyses which were not considered in the tuning procedure are described well. With the possibility of baryonic colour reconnections a lever on hadronic ratios was introduced. It was shown that the baryonic multiplicities can be improved but are still far from satisfactorily described. Especially the description of strange hadron observables lacks significantly in accuracy which indicates that the production mechanism of strangeness has to be reconsidered.

This thesis serves as the first step in rebuilding the underlying event model in Herwig 7. The new model for soft multiple parton interactions will be part of the new release, Herwig 7.1 and it will be interesting to see its application in analyses. The new model for colour reconnection will probably find its way into Herwig 7 in the near future. Ongoing

work is also considered with a dynamical approach to colour reconnection with input from a perturbative point of view.

Although the effects of colour reconnection on the new model are less significant in terms of reduction of invariant cluster mass, colour reconnection still seems to be indispensable in order to describe data from hadronic collisions. The onset of the $\langle p_{\perp} \rangle(N_{\text{ch}})$ observables remains difficult to describe for a low cut on p_{\perp} .

With the end of the data taking period of LHC run 2 we are confident that more 13 TeV analyses concerned with the underlying event will be available soon. With these analyses we will get further insights of the intricacies of our new models and are hopeful to solve ongoing issues.

Bibliography

- [1] Johannes Bellm et al. “Herwig 7.0/Herwig++ 3.0 release note”. In: *Eur. Phys. J. C* 76.4 (2016), p. 196. DOI: 10.1140/epjc/s10052-016-4018-8. arXiv: 1512.01178 [hep-ph].
- [2] T. Regge. “Introduction to complex orbital momenta”. In: *Il Nuovo Cimento (1955-1965)* 14.5 (1959), pp. 951–976. ISSN: 1827-6121. DOI: 10.1007/BF02728177. URL: <http://dx.doi.org/10.1007/BF02728177>.
- [3] Serguei Chatrchyan et al. “Observation of a new boson at a mass of 125 GeV with the CMS experiment at the LHC”. In: *Phys. Lett. B* 716 (2012), pp. 30–61. DOI: 10.1016/j.physletb.2012.08.021. arXiv: 1207.7235 [hep-ex].
- [4] Georges Aad et al. “Observation of a new particle in the search for the Standard Model Higgs boson with the ATLAS detector at the LHC”. In: *Phys. Lett. B* 716 (2012), pp. 1–29. DOI: 10.1016/j.physletb.2012.08.020. arXiv: 1207.7214 [hep-ex].
- [5] David J. Gross and Frank Wilczek. “Ultraviolet Behavior of Non-Abelian Gauge Theories”. In: *Phys. Rev. Lett.* 30 (26 1973), pp. 1343–1346. DOI: 10.1103/PhysRevLett.30.1343. URL: <http://link.aps.org/doi/10.1103/PhysRevLett.30.1343>.
- [6] H. David Politzer. “Reliable Perturbative Results for Strong Interactions?” In: *Phys. Rev. Lett.* 30 (1973), pp. 1346–1349. DOI: 10.1103/PhysRevLett.30.1346.
- [7] P. A. Baikov, K. G. Chetyrkin, and J. H. Kühn. “Five-Loop Running of the QCD coupling constant”. In: (2016). arXiv: 1606.08659 [hep-ph].
- [8] Jeffrey R. Forshaw and D. A. Ross. “Quantum chromodynamics and the pomeron”. In: *Cambridge Lect. Notes Phys.* 9 (1997), pp. 1–248.
- [9] Geoffrey F. Chew and Steven C. Frautschi. “Regge Trajectories and the Principle of Maximum Strength for Strong Interactions”. In: *Phys. Rev. Lett.* 8 (1 1962), pp. 41–44. DOI: 10.1103/PhysRevLett.8.41. URL: <http://link.aps.org/doi/10.1103/PhysRevLett.8.41>.
- [10] I Ya Pomeranchuk et al. “High Energy Collisions of Elementary Particles”. In: *Zh. Eksp. Teor. Fiz* 30 (1956), p. 423.

- [11] A. Donnachie and P. V. Landshoff. “Total cross-sections”. In: *Phys. Lett.* B296 (1992), pp. 227–232. DOI: 10.1016/0370-2693(92)90832-0. arXiv: hep-ph/9209205 [hep-ph].
- [12] D. Amati, A. Stanghellini, and S. Fubini. “Theory of high-energy scattering and multiple production”. In: *Il Nuovo Cimento (1955-1965)* 26.5 (1962), pp. 896–954. ISSN: 1827-6121. DOI: 10.1007/BF02781901. URL: <http://dx.doi.org/10.1007/BF02781901>.
- [13] M. Baker and K.A. Ter-Martirosyan. “Gribov’s Reggeon calculus: Its physical basis and implications”. In: *Physics Reports* 28.1 (1976), pp. 1–143. ISSN: 0370-1573. DOI: [http://dx.doi.org/10.1016/0370-1573\(76\)90002-8](http://dx.doi.org/10.1016/0370-1573(76)90002-8). URL: <http://www.sciencedirect.com/science/article/pii/0370157376900028>.
- [14] A.B. Kaidalov. “Diffractive production mechanisms”. In: *Physics Reports* 50.3 (1979), pp. 157–226. ISSN: 0370-1573. DOI: [http://dx.doi.org/10.1016/0370-1573\(79\)90043-7](http://dx.doi.org/10.1016/0370-1573(79)90043-7). URL: <http://www.sciencedirect.com/science/article/pii/0370157379900437>.
- [15] Christian. Roehr. “simulation of soft Inclusive Events at Hadron Colliders”. In: *PhD thesis* (2014). URL: <https://publikationen.bibliothek.kit.edu/1000039423..>
- [16] J. Alwall et al. “The automated computation of tree-level and next-to-leading order differential cross sections, and their matching to parton shower simulations”. In: *JHEP* 07 (2014), p. 079. DOI: 10.1007/JHEP07(2014)079. arXiv: 1405.0301 [hep-ph].
- [17] J. Baglio et al. “Release Note - VBFNLO 2.7.0”. In: (2014). arXiv: 1404.3940 [hep-ph].
- [18] Johan Alwall et al. “A Standard format for Les Houches event files”. In: *Comput. Phys. Commun.* 176 (2007), pp. 300–304. DOI: 10.1016/j.cpc.2006.11.010. arXiv: hep-ph/0609017 [hep-ph].
- [19] Andy Buckley et al. “General-purpose event generators for LHC physics”. In: *Phys. Rept.* 504 (2011), pp. 145–233. DOI: 10.1016/j.physrep.2011.03.005. arXiv: 1101.2599 [hep-ph].
- [20] Stefan Gieseke, P. Stephens, and Bryan Webber. “New formalism for QCD parton showers”. In: *JHEP* 12 (2003), p. 045. DOI: 10.1088/1126-6708/2003/12/045. arXiv: hep-ph/0310083 [hep-ph].
- [21] G’t Hooft. “A planar diagram theory for strong interactions”. In: *Nuclear Physics B* 72.3 (1974), pp. 461–473. ISSN: 0550-3213. DOI: [http://dx.doi.org/10.1016/0550-3213\(74\)90154-0](http://dx.doi.org/10.1016/0550-3213(74)90154-0). URL: <http://www.sciencedirect.com/science/article/pii/0550321374901540>.

- [22] S. Catani and M. H. Seymour. “A General algorithm for calculating jet cross-sections in NLO QCD”. In: *Nucl. Phys.* B485 (1997). [Erratum: *Nucl. Phys.*B510,503(1998)], pp. 291–419. DOI: 10.1016/S0550-3213(96)00589-5, 10.1016/S0550-3213(98)81022-5. arXiv: hep-ph/9605323 [hep-ph].
- [23] B.R. Webber. “A QCD model for jet fragmentation including soft gluon interference”. In: *Nuclear Physics B* 238.3 (1984), pp. 492–528. ISSN: 0550-3213. DOI: [http://dx.doi.org/10.1016/0550-3213\(84\)90333-X](http://dx.doi.org/10.1016/0550-3213(84)90333-X). URL: <http://www.sciencedirect.com/science/article/pii/055032138490333X>.
- [24] D. Amati and G. Veneziano. “Preconfinement as a property of perturbative QCD”. In: *Physics Letters B* 83.1 (1979), pp. 87–92. ISSN: 0370-2693. DOI: [http://dx.doi.org/10.1016/0370-2693\(79\)90896-7](http://dx.doi.org/10.1016/0370-2693(79)90896-7). URL: <http://www.sciencedirect.com/science/article/pii/0370269379908967>.
- [25] J. M. Butterworth, Jeffrey R. Forshaw, and M. H. Seymour. “Multiparton interactions in photoproduction at HERA”. In: *Z. Phys.* C72 (1996), pp. 637–646. DOI: 10.1007/BF02909195, 10.1007/s002880050286. arXiv: hep-ph/9601371 [hep-ph].
- [26] Loyal Durand and Hong Pi. “High-energy nucleon-nucleus scattering and cosmic-ray cross sections”. In: *Phys. Rev. D* 38 (1 1988), pp. 78–84. DOI: 10.1103/PhysRevD.38.78. URL: <http://link.aps.org/doi/10.1103/PhysRevD.38.78>.
- [27] I. Borozan and M. H. Seymour. “An Eikonal model for multiparticle production in hadron hadron interactions”. In: *JHEP* 09 (2002), p. 015. DOI: 10.1088/1126-6708/2002/09/015. arXiv: hep-ph/0207283 [hep-ph].
- [28] Loyal Durand and Hong Pi. “Semihard QCD and high-energy pp and $\bar{p}p$ scattering”. In: *Phys. Rev. D* 40 (5 1989), pp. 1436–1445. DOI: 10.1103/PhysRevD.40.1436. URL: <http://link.aps.org/doi/10.1103/PhysRevD.40.1436>.
- [29] Manuel Bahr, Jonathan M. Butterworth, and Michael H. Seymour. “The Underlying Event and the Total Cross Section from Tevatron to the LHC”. In: *JHEP* 01 (2009), p. 065. DOI: 10.1088/1126-6708/2009/01/065. arXiv: 0806.2949 [hep-ph].
- [30] Manuel Bahr et al. “Soft interactions in Herwig++”. In: *Proceedings, 1st International Workshop on Multiple Partonic Interactions at the LHC (MPI08): Perugia, Italy, October 27-31, 2008*. 2009, pp. 239–248. arXiv: 0905.4671 [hep-ph]. URL: <https://inspirehep.net/record/821555/files/arXiv:0905.4671.pdf>.
- [31] M. Bahr et al. “Herwig++ Physics and Manual”. In: *Eur. Phys. J.* C58 (2008), pp. 639–707. DOI: 10.1140/epjc/s10052-008-0798-9. arXiv: 0803.0883 [hep-ph].

- [32] Manuel Bahr. “Underlying Event Simulation in the Herwig+ Event Generator”. In: *PhD thesis* (2008). URL: <http://digbib.ubka.uni-karlsruhe.de/volltexte/1000010075..>
- [33] Paolo Lipari and Maurizio Lusignoli. “Multiple Parton Interactions in Hadron Collisions and Diffraction”. In: *Phys. Rev. D* 80 (2009), p. 074014. DOI: 10.1103/PhysRevD.80.074014. arXiv: 0908.0495 [hep-ph].
- [34] Richard Corke and Torbjorn Sjostrand. “Multiparton Interactions with an x-dependent Proton Size”. In: *JHEP* 05 (2011), p. 009. DOI: 10.1007/JHEP05(2011)009. arXiv: 1101.5953 [hep-ph].
- [35] Jeffrey R. Forshaw and J. K. Storrow. “On the interpretation of the HERA total cross-section measurement”. In: (1993).
- [36] Affolder et al. “Charged jet evolution and the underlying event in proton-antiproton collisions at 1.8 TeV”. In: *Phys. Rev. D* 65 (9 2002), p. 092002. DOI: 10.1103/PhysRevD.65.092002. URL: <http://link.aps.org/doi/10.1103/PhysRevD.65.092002>.
- [37] Stefan Gieseke, Christian Rohr, and Andrzej Siodmok. “Colour reconnections in Herwig++”. In: *Eur. Phys. J. C* 72 (2012), p. 2225. DOI: 10.1140/epjc/s10052-012-2225-5. arXiv: 1206.0041 [hep-ph].
- [38] G. Aad et al. “Charged-particle multiplicities in pp interactions measured with the ATLAS detector at the LHC”. In: *New J. Phys.* 13 (2011), p. 053033. DOI: 10.1088/1367-2630/13/5/053033. arXiv: 1012.5104 [hep-ex].
- [39] *Towards Diffraction in Herwig*. 2016, pp. 53–57. arXiv: 1602.04690 [hep-ph]. URL: <https://inspirehep.net/record/1421665/files/arXiv:1602.04690.pdf>.
- [40] Georges Aad et al. “Rapidity gap cross sections measured with the ATLAS detector in pp collisions at $\sqrt{s} = 7$ TeV”. In: *Eur. Phys. J. C* 72 (2012), p. 1926. DOI: 10.1140/epjc/s10052-012-1926-0. arXiv: 1201.2808 [hep-ex].
- [41] John C. Collins. “Light cone variables, rapidity and all that”. In: (1997). arXiv: hep-ph/9705393 [hep-ph].
- [42] Manuel Bahr, Stefan Gieseke, and Michael H. Seymour. “Simulation of multiple partonic interactions in Herwig++”. In: *JHEP* 07 (2008), p. 076. DOI: 10.1088/1126-6708/2008/07/076. arXiv: 0803.3633 [hep-ph].
- [43] Andy Buckley et al. “Systematic event generator tuning for the LHC”. In: *Eur. Phys. J. C* 65 (2010), pp. 331–357. DOI: 10.1140/epjc/s10052-009-1196-7. arXiv: 0907.2973 [hep-ph].

-
- [44] Andy Buckley et al. “Rivet user manual”. In: *Comput. Phys. Commun.* 184 (2013), pp. 2803–2819. DOI: 10.1016/j.cpc.2013.05.021. arXiv: 1003.0694 [hep-ph].
- [45] Vardan Khachatryan et al. “Measurement of diffraction dissociation cross sections in pp collisions at $\sqrt{s} = 7$ TeV”. In: *Phys. Rev. D* 92.1 (2015), p. 012003. DOI: 10.1103/PhysRevD.92.012003. arXiv: 1503.08689 [hep-ex].
- [46] Vardan Khachatryan et al. “Charged particle multiplicities in pp interactions at $\sqrt{s} = 0.9, 2.36,$ and 7 TeV”. In: *JHEP* 01 (2011), p. 079. DOI: 10.1007/JHEP01(2011)079. arXiv: 1011.5531 [hep-ex].
- [47] Torbjorn Sjostrand, Stephen Mrenna, and Peter Z. Skands. “PYTHIA 6.4 Physics and Manual”. In: *JHEP* 05 (2006), p. 026. DOI: 10.1088/1126-6708/2006/05/026. arXiv: hep-ph/0603175 [hep-ph].
- [48] Vardan Khachatryan et al. “Transverse-momentum and pseudorapidity distributions of charged hadrons in pp collisions at $\sqrt{s} = 7$ TeV”. In: *Phys. Rev. Lett.* 105 (2010), p. 022002. DOI: 10.1103/PhysRevLett.105.022002. arXiv: 1005.3299 [hep-ex].
- [49] Georges Aad et al. “Charged-particle distributions in $\sqrt{s}=13$ TeV pp interactions measured with the ATLAS detector at the LHC”. In: *Phys. Lett. B* 758 (2016), pp. 67–88. DOI: 10.1016/j.physletb.2016.04.050. arXiv: 1602.01633 [hep-ex].
- [50] Gösta Gustafson, Ulf Pettersson, and P.M. Zerwas. “Jet final states in WW pair production and colour screening in the QCD vacuum”. In: *Physics Letters B* 209.1 (1988), pp. 90–94. ISSN: 0370-2693. DOI: [http://dx.doi.org/10.1016/0370-2693\(88\)91836-9](http://dx.doi.org/10.1016/0370-2693(88)91836-9). URL: <http://www.sciencedirect.com/science/article/pii/0370269388918369>.
- [51] Torbjorn Sjostrand and Valery A. Khoze. “On Color rearrangement in hadronic W+ W- events”. In: *Z. Phys. C* 62 (1994), pp. 281–310. DOI: 10.1007/BF01560244. arXiv: hep-ph/9310242 [hep-ph].
- [52] Vardan Khachatryan et al. “Strange Particle Production in pp Collisions at $\sqrt{s} = 0.9$ and 7 TeV”. In: *JHEP* 05 (2011), p. 064. DOI: 10.1007/JHEP05(2011)064. arXiv: 1102.4282 [hep-ex].
- [53] Jesper R. Christiansen and Peter Z. Skands. “String Formation Beyond Leading Colour”. In: *JHEP* 08 (2015), p. 003. DOI: 10.1007/JHEP08(2015)003. arXiv: 1505.01681 [hep-ph].

- [54] Nicholas Metropolis et al. “Equation of State Calculations by Fast Computing Machines”. In: *The Journal of Chemical Physics* 21.6 (1953), pp. 1087–1092. DOI: <http://dx.doi.org/10.1063/1.1699114>. URL: <http://scitation.aip.org/content/aip/journal/jcp/21/6/10.1063/1.1699114>.
- [55] P. Abreu et al. “Tuning and test of fragmentation models based on identified particles and precision event shape data”. In: *Z. Phys. C* 73 (1996), pp. 11–60. DOI: 10.1007/s002880050295.
- [56] Jaroslav Adam et al. “Measurement of pion, kaon and proton production in proton–proton collisions at $\sqrt{s} = 7$ TeV”. In: *Eur. Phys. J. C* 75.5 (2015), p. 226. DOI: 10.1140/epjc/s10052-015-3422-9. arXiv: 1504.00024 [nucl-ex].
- [57] V. Barone and E. Predazzi. *High-Energy Particle Diffraction*. Springer, 2002. ISBN: 9783540421078.

A. Tuning

The following plots show the tuning results of the outcome of the tuning procedure for the five tuned parameters in Sec. 5.3 for 900 GeV and 7 TeV in comparison.

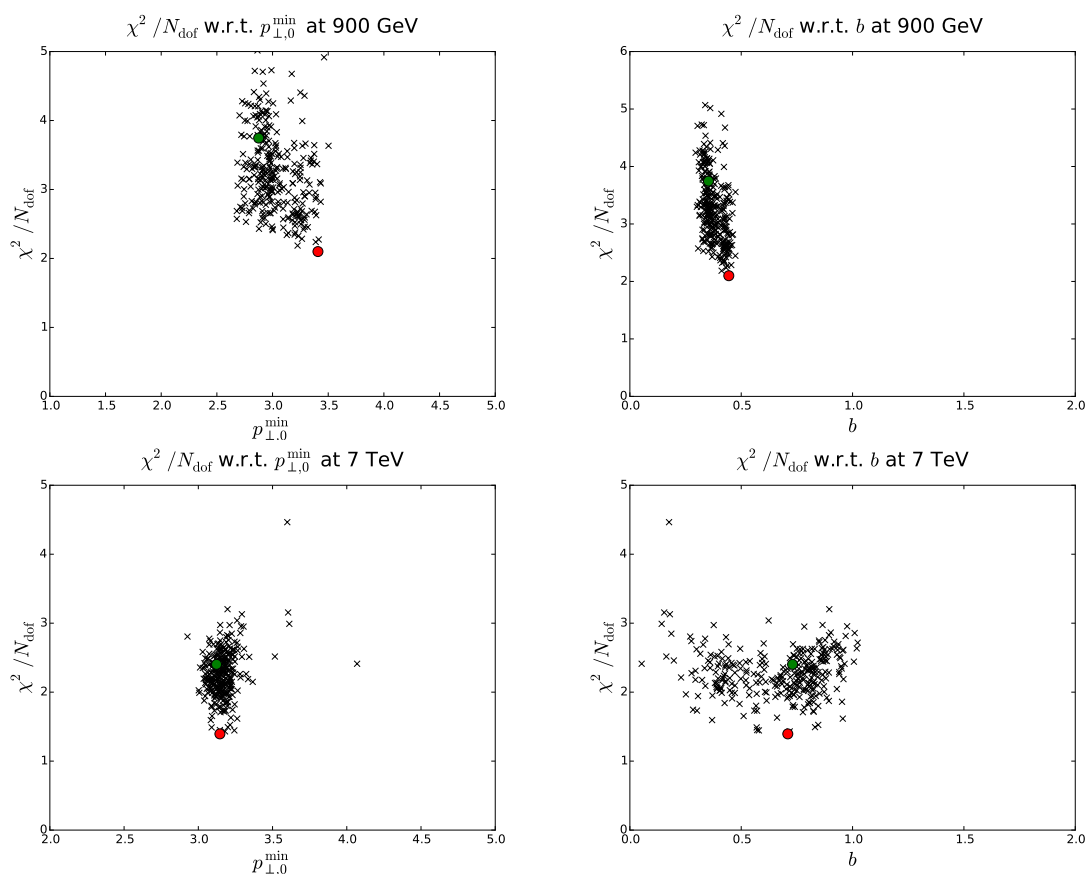


Figure A.1.: Scatterplots of the tuning results for different subsets of generator runs (black crosses) or of all generator runs (green dot). The red dot marks the minimum value of χ^2 / N_{dof} .

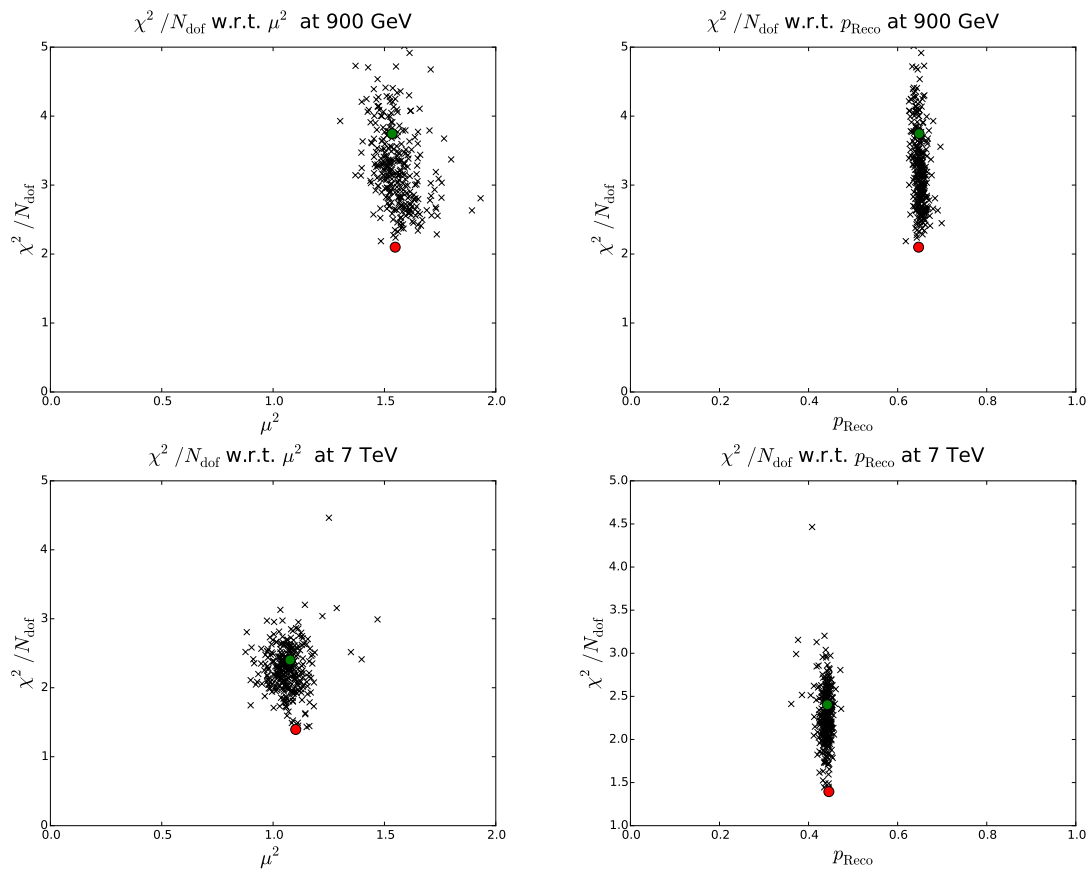


Figure A.2.: Scatterplots of the tuning results for different subsets of generator runs (black crosses) or of all generator runs (green dot). The red circle dot the minimum value of χ^2/N_{dof} .

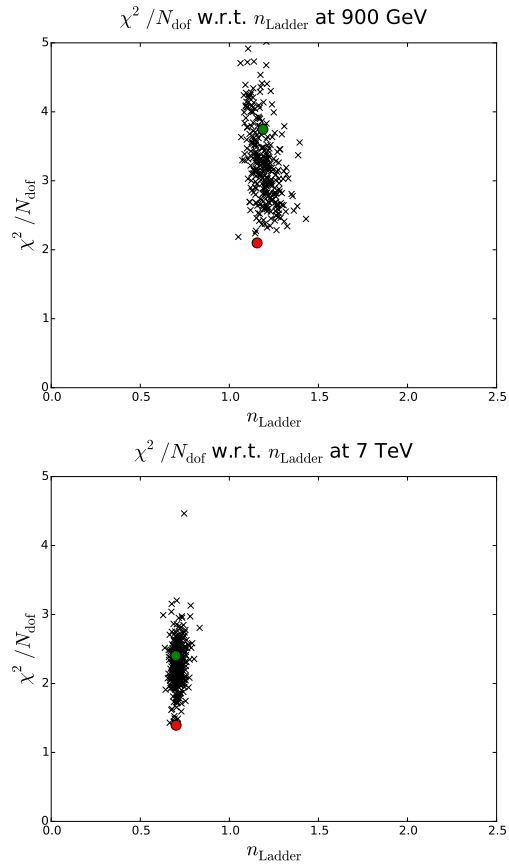


Figure A.3.: Scatterplots of the tuning results for different subsets of generator runs (black crosses) or of all generator runs (green dot). The red dot marks the minimum value of χ^2 / N_{dof} .

B. Eikonal approximation

Here we describe the eikonal approximation of a quantum mechanical amplitude following Ref. [57]. In the high energy limit of non relativistic potential scattering, the scattering amplitude can be simplified using the eikonal approximation. The Starting point is the Schrödinger equation

$$\left[\nabla^2 - U(\mathbf{r}) + k^2 \right] \Psi(\mathbf{r}) = 0 , \quad (\text{B.1})$$

which describes the motion of two spinless particles that interact via the potential $U(\mathbf{r})$. In order to solve the equation we use the ansatz for a plane wave moving in forward direction

$$\Psi(\mathbf{r}) = \phi(\mathbf{r}) e^{i\mathbf{k}\cdot\mathbf{r}} , \quad (\text{B.2})$$

where $\phi(\mathbf{r})$ is some unknown function. With the following two assumptions: *i*) The energy of the particle is much larger than the interaction potential, $E \gg |U(r)|$. *ii*) The wavelength of the particle is much smaller than the interaction range, $ka \gg 1$, the particle is scattered predominantly at small angles. Inserting the ansatz into the Schrödinger equation Eq. (B.1) leads to

$$\left(\nabla^2 + 2i\mathbf{k}\nabla - U \right) \phi(\mathbf{r}) = 0 . \quad (\text{B.3})$$

If we assume that the wave comes from $-\infty$ and that at high energies ψ and U are smooth functions of r , the term $\nabla^2\phi$ can be neglected and Eq. (B.3) simplifies to

$$[2ik\partial_z - U(x, y, z)] \phi(x, y, z) = 0 , \quad (\text{B.4})$$

where we used $\mathbf{k} = k\hat{e}_z$. This equation can be solved by

$$\phi(x, y, z) = \exp \left[-\frac{i}{2k} \int_{-\infty}^z U(x, y, z') dz' \right] . \quad (\text{B.5})$$

Inserting $\phi(x, y, z)$ into the ansatz (B.2) for Ψ , we obtain

$$\Psi(x, y, z) = \exp \left[ikz - \frac{i}{2k} \int_{-\infty}^z U(x, y, z') dz' \right] . \quad (\text{B.6})$$

Eq. (B.6) can be written in a more customary way using the impact parameter representation $\mathbf{r} = \mathbf{b} + z\hat{\mathbf{e}}_z$, where \mathbf{b} is the impact parameter. We fix the wavevector \mathbf{k} in the direction of the z-axis ($\mathbf{k} = k\hat{\mathbf{e}}_z$), and rewrite Eq. (B.6) as

$$\Psi(\mathbf{r}) = \exp \left[i\mathbf{k} \cdot \mathbf{r} - \frac{i}{2k} \int_{-\infty}^z U(\mathbf{b}, z') dz' \right]. \quad (\text{B.7})$$

Now the scattering amplitude $f(\mathbf{k}, \mathbf{k}')$ can be calculated from the formula

$$f(\mathbf{k}, \mathbf{k}') = -\frac{1}{4\pi} \int e^{i\mathbf{k}' \cdot \mathbf{r}} U(\mathbf{r}') \Psi(\mathbf{r}') d^3\mathbf{r}', \quad (\text{B.8})$$

which leads to

$$f(\mathbf{k}, \mathbf{k}') = -\frac{1}{4\pi} \int_{-\infty}^{\infty} dz \int d^2\mathbf{b} e^{-i(\mathbf{k}' - \mathbf{k}) \cdot (\mathbf{b} + z\hat{\mathbf{e}}_z)} U(\mathbf{b}, z) \times \exp \left[-\frac{i}{2k} \int_{-\infty}^z U(\mathbf{b}, z') dz' \right]. \quad (\text{B.9})$$

For small angles, $k = k'$ is valid and the momentum transfer is expressed as $\mathbf{q} = \mathbf{k}' - \mathbf{k}$. Where the modulo of \mathbf{q} is $q = 2k \sin(\frac{\theta}{2})$. Because \mathbf{q} is almost orthogonal to \mathbf{k} we can use $\mathbf{q} \cdot \mathbf{r} \approx \mathbf{q} \cdot \mathbf{b}$. With these relations, Eq. (B.9) reduces to

$$f(k, \theta, \psi) = -\frac{1}{4} \int_{-\infty}^{\infty} dz \int d^2\mathbf{b} e^{-i\mathbf{q} \cdot \mathbf{b}} U(\mathbf{b}, z) \times \exp \left[-\frac{i}{2k} \int_{-\infty}^z U(\mathbf{b}, z') dz' \right]. \quad (\text{B.10})$$

The integration over z can be performed using the identity

$$2ik \frac{\partial}{\partial z} \exp \left[-\frac{i}{2k} \int_{-\infty}^z U dz' \right] = U \exp \left[-\frac{i}{2k} \int_{-\infty}^z U dz' \right], \quad (\text{B.11})$$

and we obtain a function for the amplitude defined in terms of the two dimensional integration over the impact parameter \mathbf{b} ,

$$f(k, \theta, \psi) = \frac{ik}{2\pi} \int d^2\mathbf{b} e^{-i\mathbf{q} \cdot \mathbf{b}} (1 - e^{i\chi(\mathbf{b})}), \quad (\text{B.12})$$

where χ in Eq. (B.12) is referred to as the *eikonal function* and reads

$$\chi(\mathbf{b}) = -\frac{1}{2k} \int_{-\infty}^{+\infty} U(\mathbf{b}, z) dz. \quad (\text{B.13})$$

The total cross section σ_{tot} consists of an elastic and an inelastic contribution

$$\sigma_{\text{tot}} = \sigma_{\text{el}} + \sigma_{\text{inel}}. \quad (\text{B.14})$$

From the formula for the elastic cross section $\frac{d\sigma_{\text{el}}}{d\Omega} = |f(k, \theta, \psi)|^2$ we obtain,

$$\sigma_{\text{el}} = \int d^2\mathbf{b} |1 - e^{i\chi(\mathbf{b})}|^2 \quad (\text{B.15})$$

and with the optical theorem, that relates the total cross section σ_{tot} to the imaginary part of the forward elastic amplitude, follows

$$\sigma_{\text{tot}} = 2 \int d^2\mathbf{b} \Re(1 - e^{i\chi(\mathbf{b})}). \quad (\text{B.16})$$

Combining the total and the elastic cross sections, Eqs. (B.16,B.15), one immediately obtains a relation for the inelastic cross section σ_{inel}

$$\sigma_{\text{inel}} = \int d^2\mathbf{b} \left[2\Re(1 - e^{i\chi(\mathbf{b})}) - |1 - e^{i\chi(\mathbf{b})}|^2 \right]. \quad (\text{B.17})$$

Danksagung

Zunächst möchte ich mich bei Dr. Stefan Gieseke für die Betreuung dieser Arbeit bedanken. Ich konnte in unzähligen Diskussionen viel von ihm lernen und bin bei ihm immer auf offene Ohren gestoßen. Ich bin außerdem sehr dankbar, dass er mir die Möglichkeit gegeben hat am MCnet Meeting in Göttingen und an einem Workshop teilzunehmen.

Ich bedanke mich bei Prof. Dr. Dieter Zeppenfeld herzlich für die Übernahme des Korreferats.

Meinen besonderen Dank möchte ich Dr. Frashër Loshaj für die vielen Diskussionen, Tipps, Ratschläge und die gute Zusammenarbeit aussprechen.

Ich danke Dr. Simon Plätzer für die anregenden Diskussionen während den Meetings.

Meinen besonderen Dank verdienen auch Konstantin Asteriadis, Tobias Mistele und Florian Herren für das Korrekturlesen dieser Arbeit.

Ich danke allen Institutsmitgliedern für die außergewöhnliche und freundliche Atmosphäre während des vergangenen Jahres.

Schließlich bedanke ich mich bei meinen Eltern ohne deren Unterstützung mein Studium nicht möglich gewesen wäre.